Hindawi Publishing Corporation
Mathematical Problems in Engineering
Volume 2014, Article ID 145780, 24 pages
http://dx.doi.org/10.1155/2014/145780

Research Article

A Variational Level Set Model Combined with FCMS for Image Clustering Segmentation

Liming Tang

College of Mathematics and Physics, Chongqing University of Science and Technology, Chongqing 401331, China

Correspondence should be addressed to Liming Tang; tlmcs78@foxmail.com

Received 11 October 2013; Revised 2 January 2014; Accepted 3 January 2014; Published 23 February 2014

Academic Editor: Dan Simon

The fuzzy C means clustering algorithm with spatial constraint (FCMS) is effective for image segmentation. However, it lacks essential smoothing constraints to the cluster boundaries and enough robustness to the noise. Samson et al. proposed a variational level set model for image clustering segmentation, which can get the smooth cluster boundaries and closed cluster regions due to the use of level set scheme. However it is very sensitive to the noise since it is actually a hard C means clustering model. In this paper, based on Samson's work, we propose a new variational level set model combined with FCMS for image clustering segmentation. Compared with FCMS clustering, the proposed model can get smooth cluster boundaries and closed cluster regions due to the use of level set scheme. In addition, a block-based energy is incorporated into the energy functional, which enables the proposed model to be more robust to the noise than FCMS clustering and Samson's model. Some experiments on the synthetic and real images are performed to assess the performance of the proposed model. Compared with some classical image segmentation models, the proposed model has a better performance for the images contaminated by different noise levels.

1. Introduction

Image segmentation is separating the image domain into dissimilar homogeneous regions, which is the precondition and foundation of further image analysis and understanding. The quality of segmentation affects the result of the following analysis and processing directly. So, it is an important technique in image processing and has drawn much research attention at the theory and application. In recent years, variational level set method and clustering technology have been widely exploited in image segmentation because of their good experimental performance and sound theoretical foundation.

The variational level set model used in image segmentation is formulated as follows [1–4]. The contours are first implicitly represented by the zero level set (ZLS) of a higher dimensional function, usually referred to as the level set function. And then one can obtain evolution partial differential equation (PDE) or partial differential equations (PDEs) for level set function in terms of minimizing an energy functional which typically includes the internal energy that smoothes the level set function and the external energy that aligns the ZLS with object boundaries. At last, the level set function evolves according to the evolution PDE or PDEs and thus achieves the goal for evolving the ZLS implied therein. Compared with the traditional level set method where the level set function is driven purely by PDE, in the variational level set method, the evolution PDE is obtained by minimizing energy functional. So, more prior information (e.g., texture and shape information) on the image can be conveniently taken into account into the energy functional, which makes the variational level set method have a good performance and extensive adaptability. Here, we present some classical variational level set models for image segmentation. The well-known Mumford and Shah (MS) [5] model for image segmentation has been successfully extended to a wide range of applications. But it cannot be solved directly in practice because of the nonconvexity of its functional. Recently, some improved models are proposed, such as piecewise constant model [6] proposed by Chan and Vese (CV) and region-based active contour model [7] (RBACM) proposed by Zhang et al.. In order to enhance the quality of segmentation for image with inhomogeneous intensity, Li et al. [8] proposed an implicit active contour driven by local binary fitting energy (LBF), and then Zhang et al. [9] proposed an active contour driven by local image fitting energy (LIF) which has higher computing efficiency than LBF. The models mentioned above can only be utilized for two-phase partition. Some multiphase models are proposed, such as Vese and Chan [10] proposed multiphase CV model (MCV), Gao and Yan [11] proposed multiphase local CV model (MLCV) to improve the efficiency for noisy image segmentation.

Clustering is to partition a given input dataset or image pixels into k clusters with most similarities in the same cluster and most dissimilarities between different clusters. In the last decades, the fuzzy C means clustering (FCM) [12] has been widely used in image segmentation (e.g., [13, 14]) due to its good performance and a well-grounded theory. Such a success chiefly attributes to the introduction of fuzzy membership relations between the image pixels and the cluster centers, c_i $(i = 1, \ldots, k)$. This allows the ability of FCM to be able to retain more image information than the hard C means clustering. The original FCM clustering has a good performance on segmenting the most noise-free image, but it fails to segment images contaminated by noise, outliers, and other imaging artifacts. Ahmed et al. [15] first considered the fuzzy C means with spatial constraints (FCMS), that is, incorporating the spatial information of image into the objective function, to overcome this difficulty. Afterward, some FCMS-based models were proposed to meet different research requirements. Such as Chen and Zhang [16] modified the FCMS objective function to reduce the computational complexity. They then replaced the Euclidean distance in FCMS by a kernel-induced distance and then proposed a Gaussian kernel version of FCMS, called GFCMS later. Yang and Tsai [17] proposed a generalized type of GFCMS in which the parameters can be automatically estimated under a learning scheme. Kannan et al. [18] proposed an effective FCMS for segmenting medical images. Liu et al. [19] proposed a fuzzy spectral clustering combined with spatial information. He et al. [20] proposed a new FCM clustering with total variation regularization for segmenting the images with noisy and incomplete data.

The above mentioned clustering algorithms are all based on the discrete data. They utilize the intensity, statistics properties, and spatial features of image pixels to perform pixels clustering. But they cannot obtain the smooth cluster boundaries and closed cluster regions due to the lack of the essential smoothing constraint to the cluster boundaries, while the variational level set method just can deal with the above problems. So, the image segmentation quality will be improved if the clustering algorithms are appropriately combined with the variational level set method. However, most of the current clustering algorithms are based on the discrete dataset, while variation method is based on continuous function. So, these two techniques cannot be combined together easily. Samson et al. [21] first solved this problem in 2000 by the use of level set method. As the first attempt of combining data clustering with variation method, Samson's model still has some drawbacks, such as (1) it is a hard C means clustering; (2) it is very sensitive to the noise; and (3) it is a supervised clustering model. To solve these drawbacks, we propose a variational level set model combined with FCMS clustering (called VFCMS later) in this paper. Compared with Samson's model, the proposed model has the following advantages: (1) it is a fuzzy clustering model; (2) it is very robust to the noise; and (3) it is a semisupervised clustering model.

The remainder of this paper is organized as follows: in Section 2, some backgrounds concerning the standard FCMS clustering (and its variants) and Samson's model are presented; some drawbacks of them are also mentioned. In Section 3, a variational level set model combined with FCMS (i.e., VFCMS) is proposed. In Section 4, we apply the proposed model to image clustering segmentation. The comparisons with some classical image segmentation models are also performed in this section. This paper is summarized in Section 5.

2. The Backgrounds

2.1. FCMS Clustering and Its Variants. In [15], the authors proposed FCMS clustering to partition the discrete dataset $\{\mathbf{x}_j\}_{j=1}^{n}$ into k clusters. The main contribution of FCMS is that the spatial information of the discrete dataset was incorporated into the objective function, which can increase the robustness to noise. The objective function of FCMS is defined as

$$\begin{aligned}\mathcal{J}^{\mathrm{FCMS}}\left(\mu_{ij}, \mathbf{v}_i\right) &= \sum_{i=1}^{k}\sum_{j=1}^{n}\mu_{ij}^{m}\left\|\mathbf{x}_j - \mathbf{v}_i\right\|^2 \\ &\quad + \frac{\alpha}{N_R}\sum_{i=1}^{k}\sum_{j=1}^{n}\mu_{ij}^{m}\sum_{r\in N_j}\left\|\mathbf{x}_r - \mathbf{v}_i\right\|^2, \end{aligned} \tag{1}$$

$$\text{s.t. } 0 \le \mu_{ij} \le 1; \quad \sum_{i=1}^{k}\mu_{ij} = 1, \quad \forall j; \quad \sum_{j=1}^{n}\mu_{ij} = 1, \quad \forall i,$$

where μ_{ij} is a fuzzy membership matrix and m is weighting exponent on each fuzzy membership; $\{\mathbf{v}_i\}_{i=1}^{k}$ are the cluster centers. N_j is the set of neighbors falling into the window centered at $\mathbf{x}_j$ and N_R is its cardinality; the parameter α is the weighting coefficient of the spatial constraints. In essence, the spatial constraint (the second term in (1)) aims at keeping the continuity on the neighboring data values around $\mathbf{x}_j$. By minimizing in a way similar to the standard FCM algorithm, the necessary conditions on μ_{ij} and $\mathbf{v}_i$ for (1) to be at a local minimum are

$$\begin{aligned}\mu_{ij} &= \frac{\left(\left\|\mathbf{x}_j - \mathbf{v}_i\right\|^2 + (\alpha/N_R)\sum_{r\in N_j}\left\|\mathbf{x}_r - \mathbf{v}_i\right\|^2\right)^{-1/(m-1)}}{\sum_{t=1}^{k}\left(\left\|\mathbf{x}_j - \mathbf{v}_t\right\|^2 + (\alpha/N_R)\sum_{r\in N_j}\left\|\mathbf{x}_r - \mathbf{v}_t\right\|^2\right)^{-1/(m-1)}}; \\ \mathbf{v}_i &= \frac{\sum_{j=1}^{n}\mu_{ij}^{m}\left(\mathbf{x}_j + (\alpha/N_R)\sum_{r\in N_j}\mathbf{x}_r\right)}{(1+\alpha)\sum_{j=1}^{n}\mu_{ij}^{m}}. \end{aligned} \tag{2}$$

The procedure of FCMS clustering is as follows. First, based on the prior information of dataset, predefine the cluster number k and the initial cluster centers $\{\mathbf{v}_i\}_{i=1}^{k}$. And then update the fuzzy membership matrix μ_{ij} and cluster centers

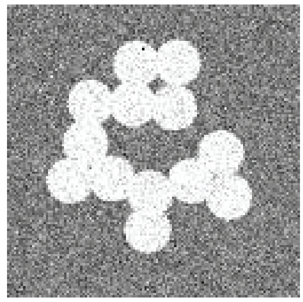

(a) Noisy data

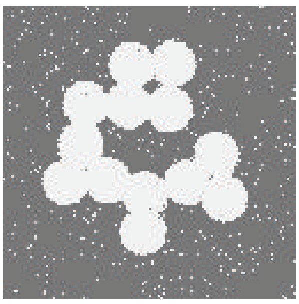

(b) FCM

(c) FCMS_1

(d) FCMS_2

(e) GFCMS

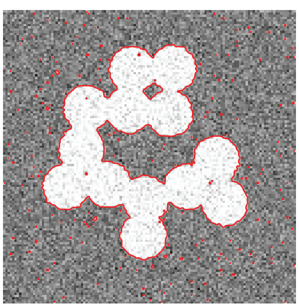

(f) CV (ZLSs)

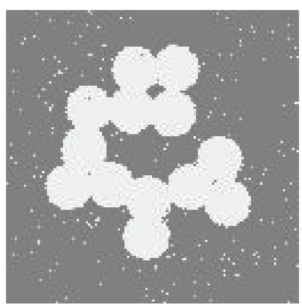

(g) CV

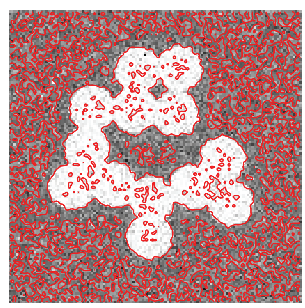

(h) LIF (ZLSs)

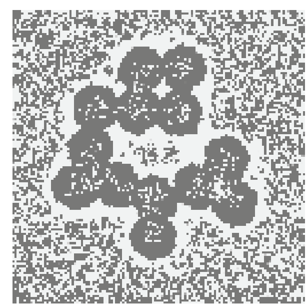

(i) LIF

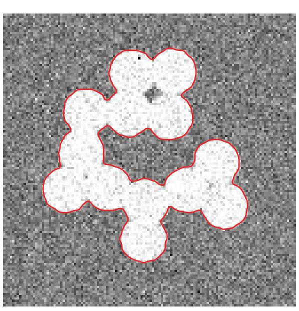

(j) RBACM (ZLSs)

(k) RBACM

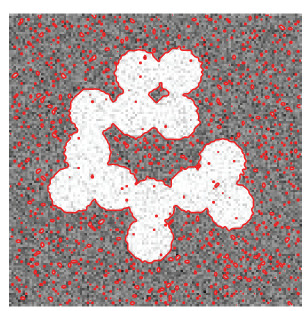

(l) Samson's model (ZLSs)

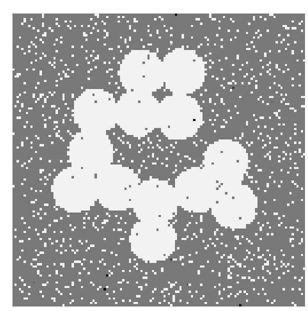

(m) Samson's model

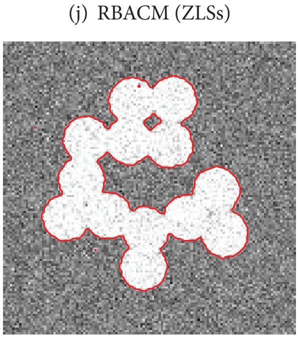

(n) VFCMS_1 (ZLSs)

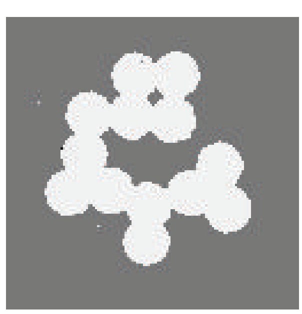

(o) VFCMS_1

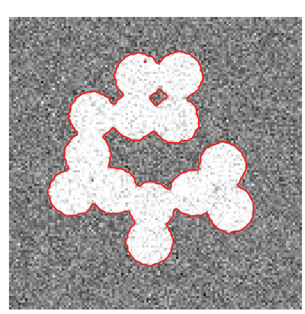

(p) VFCMS_2 (ZLSs)

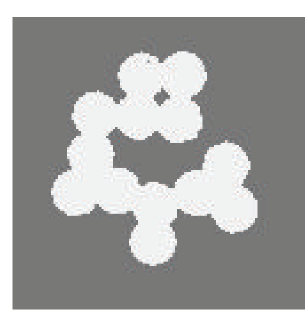

(q) VFCMS_2

Figure 1: Continued.

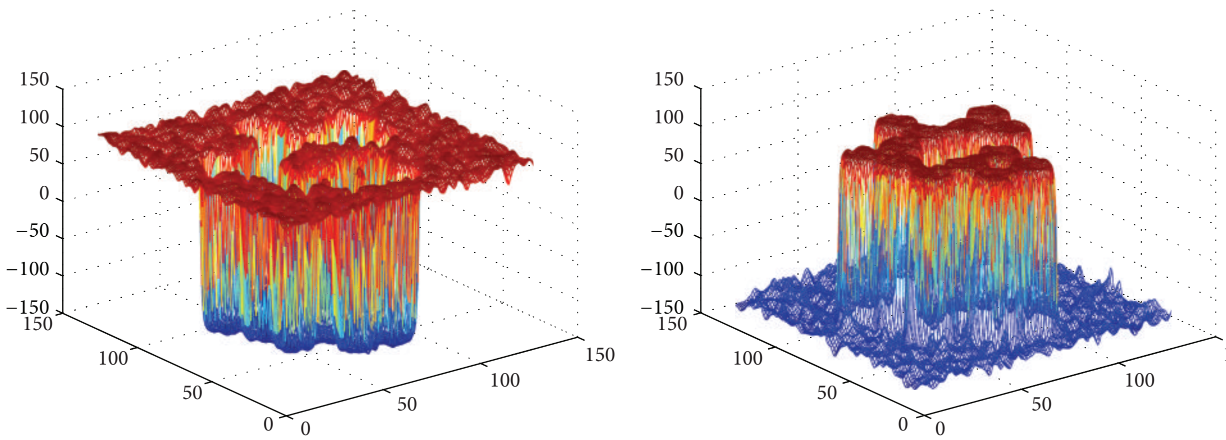

(r) The surface plot of ϕ_1

(s) The surface plot of ϕ_2

Figure 1: Comparison of segmentation results on a synthetic image with mixed 1% Salt and Pepper, Gaussian, and Speckle noise (cluster number $k = 2$).

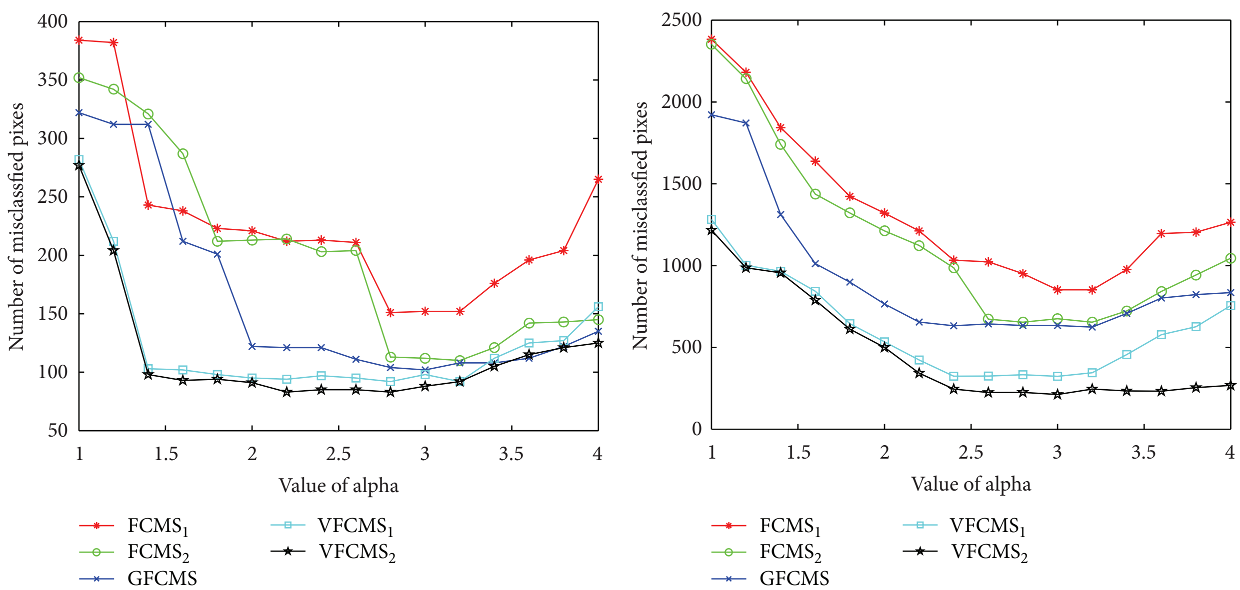

(a) Comparison of classification errors on synthetic image with 1% mixed noise under different values of alpha

(b) Comparison of classification errors on synthetic image with 2% mixed noise under different values of alpha

Figure 2: Comparison of classification errors on two-phase synthetic image with different mixed noise levels under different values of alpha.

$\{\mathbf{v}_i\}_{i=1}^{k}$ successively by (2) until $\|\mathbf{v}_{\text{new}} - \mathbf{v}_{\text{old}}\| < \varepsilon$. Then the output $\mathbf{v}_{\text{new}} = (v_1, \ldots, v_k)$ is the final clustering centers.

In [16], Chen and Zhang studied the FCMS clustering and pointed out a shortcoming of its update equations (2), that is, computing the neighborhood terms will take much more time than the classical FCM. They noticed that

$$\frac{1}{N_R}\sum_{r\in N_j}\left\|\mathbf{x}_r - \mathbf{v}_i\right\|^2 = \frac{1}{N_R}\sum_{r\in N_j}\left\|\mathbf{x}_r - \overline{\mathbf{x}}_j\right\|^2 + \left\|\overline{\mathbf{x}}_j - \mathbf{v}_i\right\|^2, \tag{3}$$

where $\overline{\mathbf{x}}_j$ is the median or mean of neighboring data lying within a window around $\mathbf{x}_j$, and then proposed a modified FCMS objective function by replacing $(1/N_R)\sum_{r\in N_j}\|\mathbf{x}_r - \mathbf{v}_i\|^2$ with $\|\overline{\mathbf{x}}_j - \mathbf{v}_i\|^2$.

$$\begin{aligned}\mathcal{J}^{\text{FCMS}}\left(\mu_{ij}, \mathbf{v}_i\right) &= \sum_{i=1}^{k}\sum_{j=1}^{n}\mu_{ij}^{m}\left\|\mathbf{x}_j - \mathbf{v}_i\right\|^2 \\ &\quad + \alpha\sum_{i=1}^{k}\sum_{j=1}^{n}\mu_{ij}^{m}\left\|\overline{\mathbf{x}}_j - \mathbf{v}_i\right\|^2,\end{aligned} \tag{4}$$

$$\text{s.t. } 0 \le u_{ij} \le 1; \quad \sum_{i=1}^{k}\mu_{ij} = 1, \quad \forall j; \quad \sum_{j=1}^{n}\mu_{ij} = 1, \quad \forall i.$$

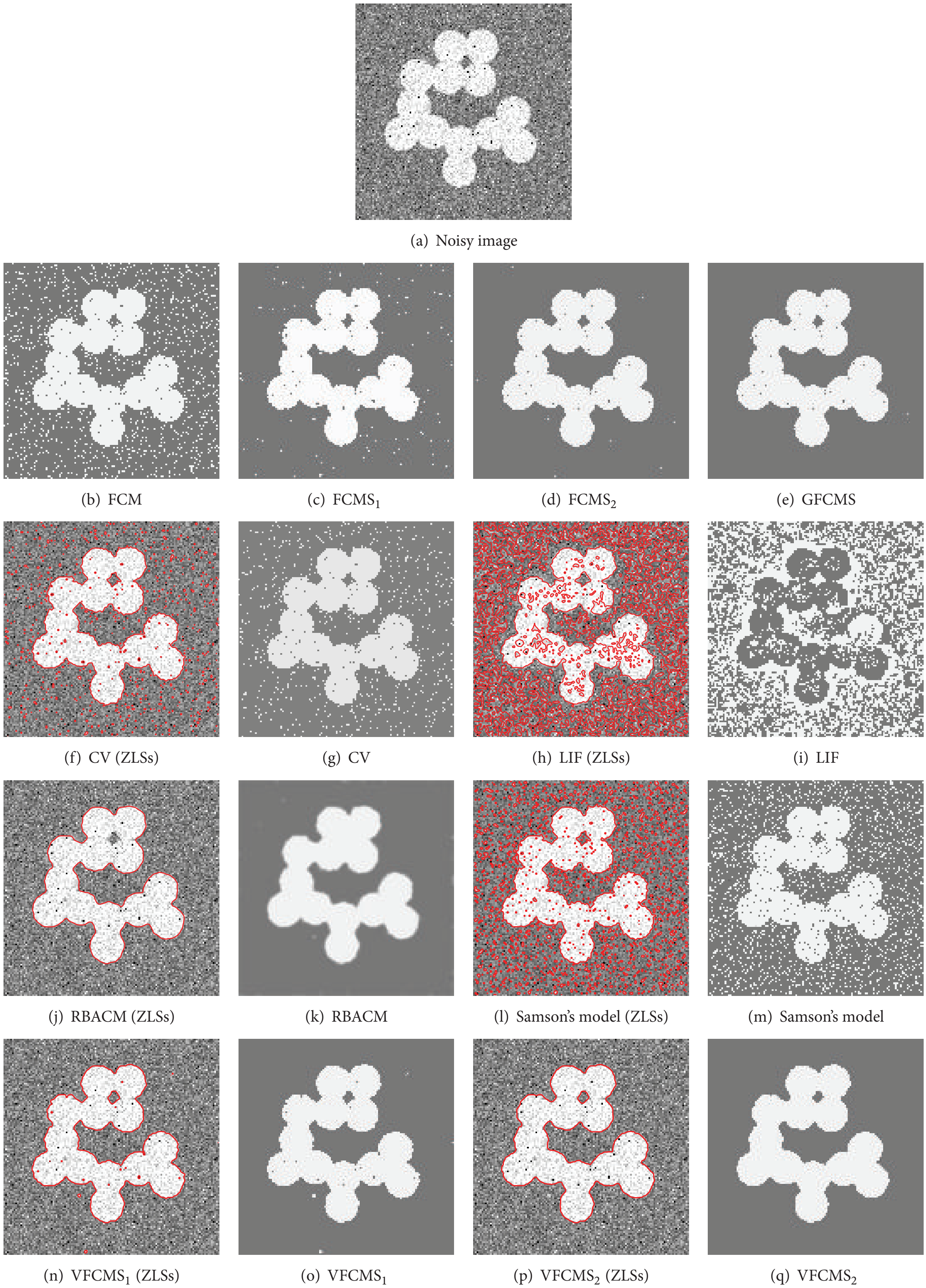

(a) Noisy image
(b) FCM
(c) $FCMS_1$
(d) $FCMS_2$
(e) GFCMS
(f) CV (ZLSs)
(g) CV
(h) LIF (ZLSs)
(i) LIF
(j) RBACM (ZLSs)
(k) RBACM
(l) Samson's model (ZLSs)
(m) Samson's model
(n) $VFCMS_1$ (ZLSs)
(o) $VFCMS_1$
(p) $VFCMS_2$ (ZLSs)
(q) $VFCMS_2$

FIGURE 3: Comparison of segmentation results on a synthetic image with mixed 2% Salt and Pepper, Gaussian, and Speckle noise (cluster number $k = 2$).

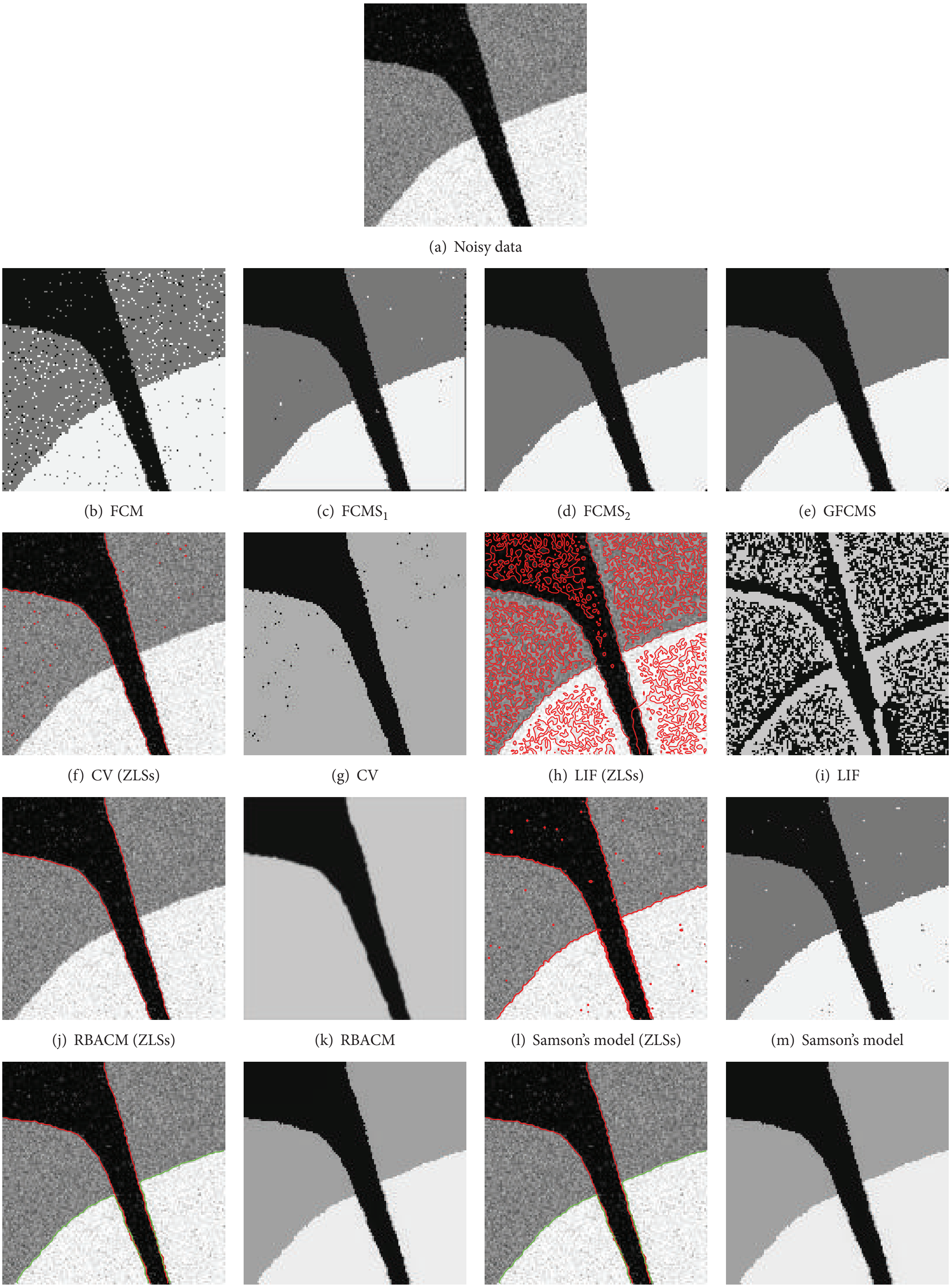

(a) Noisy data

(b) FCM

(c) $FCMS_1$

(d) $FCMS_2$

(e) GFCMS

(f) CV (ZLSs)

(g) CV

(h) LIF (ZLSs)

(i) LIF

(j) RBACM (ZLSs)

(k) RBACM

(l) Samson's model (ZLSs)

(m) Samson's model

(n) MCV (ZLSs)

(o) MCV

(p) MLCV (ZLSs)

(q) MLCV

Figure 4: Continued.

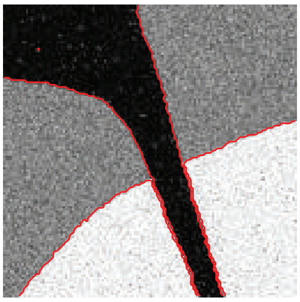

(r) VFCMS_1 (ZLSs)

(s) VFCMS_1

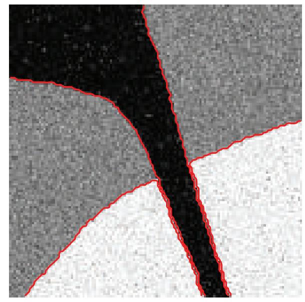

(t) VFCMS_2 (ZLSs)

(u) VFCMS_2

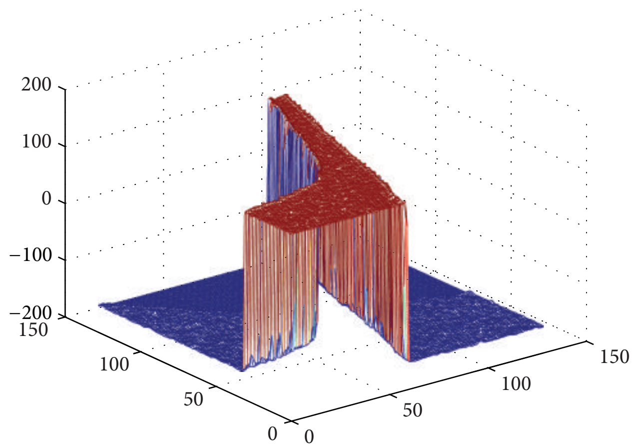

(v) The surface plot of ϕ_1

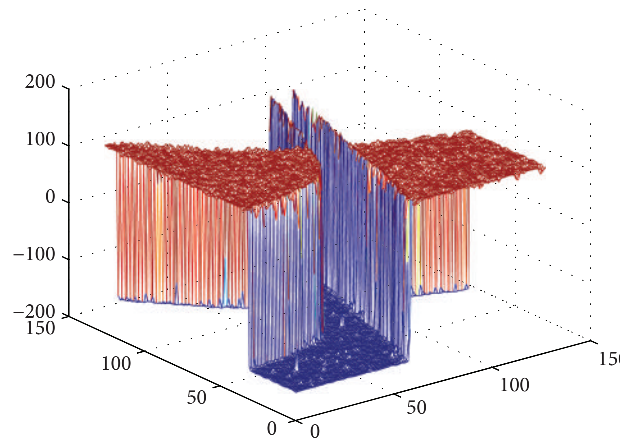

(w) The surface plot of ϕ_2

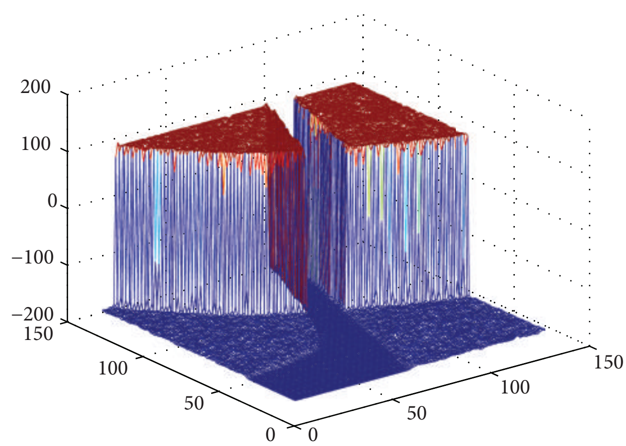

(x) The surface plot of ϕ_3

FIGURE 4: Comparison of segmentation results on a synthetic image with mixed 0.5% Salt and Pepper, Gaussian, and Speckle noise (cluster number $k = 3$).

Similarly, minimizing the $\mathcal{J}^{\mathrm{FCMS}}(\mu_{ij}^m, \mathbf{v}_i)$ in (4) with respect to μ_{ij} and $\mathbf{v}_i$, we can obtain

$$\mu_{ij} = \frac{\left(\left\|\mathbf{x}_j - \mathbf{v}_i\right\|^2 + \alpha\left\|\overline{\mathbf{x}}_j - \mathbf{v}_i\right\|^2\right)^{-1/(m-1)}}{\sum_{t=1}^{k}\left(\left\|\mathbf{x}_j - \mathbf{v}_t\right\|^2 + \alpha\left\|\overline{\mathbf{x}}_j - \mathbf{v}_t\right\|^2\right)^{-1/(m-1)}};$$
$$\mathbf{v}_i = \frac{\sum_{j=1}^{n}\mu_{ij}^m\left(\mathbf{x}_j + \alpha\overline{\mathbf{x}}_j\right)}{(1+\alpha)\sum_{j=1}^{n}\mu_{ij}^m}, \tag{5}$$

where $\overline{\mathbf{x}}_j$ can be computed in advance. Obviously, updating (5) is simpler than (2). So the clustering time can be saved. For convenience of notation, the authors of [16] named the clustering algorithm using (5) with median and mean filtering FCMS_1 and FCMS_2, respectively.

Although FCMS clustering and its variants (e.g., FCMS_1 and FCMS_2) have the benefits that it is simple and easy to manipulate, it cannot obtain the smooth cluster boundaries and the closed cluster regions for the lack of the essential smoothing constraints for the cluster boundaries. In addition,

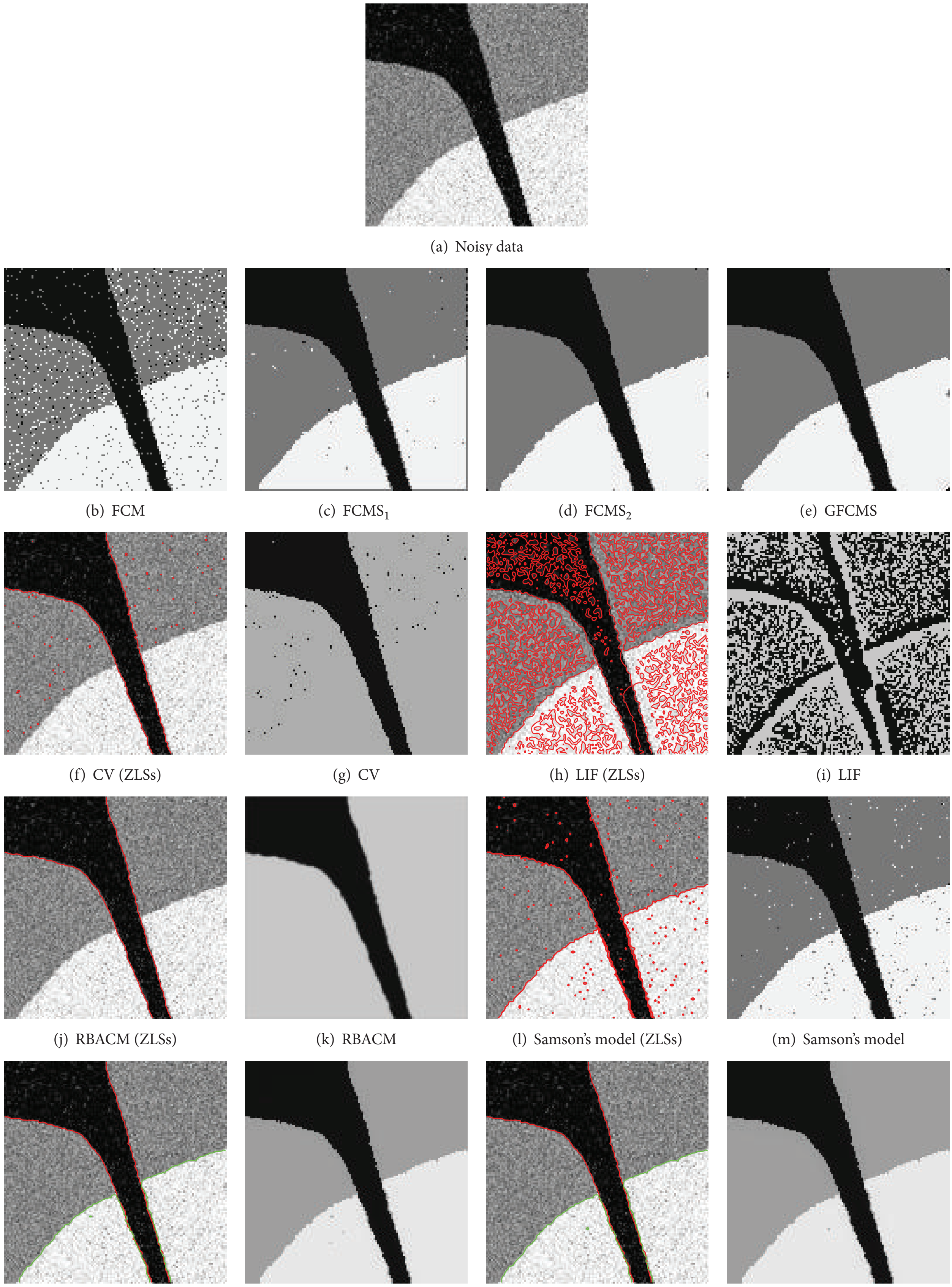

(a) Noisy data

(b) FCM

(c) $FCMS_1$

(d) $FCMS_2$

(e) GFCMS

(f) CV (ZLSs)

(g) CV

(h) LIF (ZLSs)

(i) LIF

(j) RBACM (ZLSs)

(k) RBACM

(l) Samson's model (ZLSs)

(m) Samson's model

(n) MCV (ZLSs)

(o) MCV

(p) MLCV (ZLSs)

(q) MLCV

FIGURE 5: Continued.

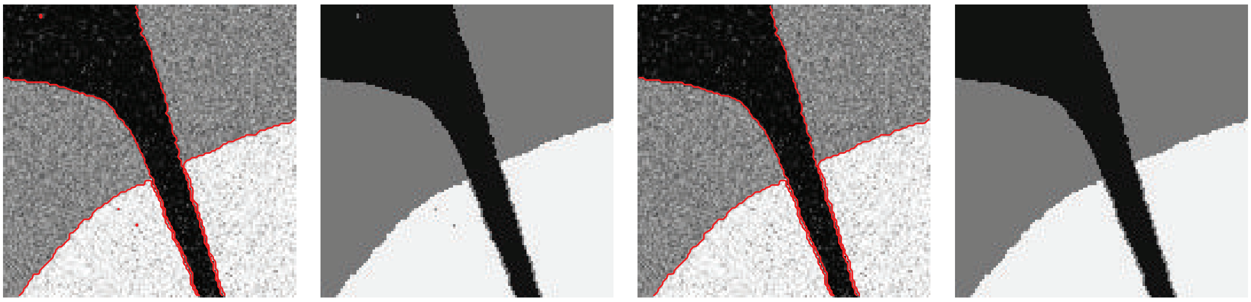

(r) VFCMS_1 (ZLSs) (s) VFCMS_1 (t) VFCMS_2 (ZLSs) (u) VFCMS_2

FIGURE 5: Comparison of segmentation results on a synthetic image with mixed 1.5% Salt and Pepper, Gaussian, and Speckle noise (cluster number $k = 3$).

although the spatial constraint is incorporated into the objective function, FCMS cannot achieve good clustering result when the dataset is contaminated by strong noise.

2.2. Samson's Model. The mentioned above clustering algorithms are all based on the discrete data, so they cannot be solved by the variational method directly. It was the first time for Samson et al. to employ the variational method for data clustering by using level set method. In [21], they proposed a clustering model based on variational level set and then applied it to image clustering segmentation. Let image domain be $\Omega \in \mathbb{R}^2$ and let image function be $f(\mathbf{x}) : \Omega \to \mathbb{R}$. Image clustering segmentation is equivalent to solving the following minimization problem:

$$\inf_{\phi_i} \Bigg\{ E(\phi_1 \cdots \phi_k) = \sum_{i=1}^{k} e_i \int_\Omega \frac{(f(\mathbf{x}) - c_i)^2}{\sigma_i} H(\phi_i(\mathbf{x}))\, d\mathbf{x} + \sum_{i=1}^{k} \gamma_i \int_\Omega g(f(\mathbf{x})) \left|\nabla H(\phi_i(\mathbf{x}))\right| d\mathbf{x} + \frac{1}{2}\kappa \int_\Omega \left(\sum_{i=1}^{k} H(\phi_i(\mathbf{x})) - 1 \right)^2 d\mathbf{x} \Bigg\}. \tag{6}$$

The first term of the energy functional (6) aims to partition the image domain Ω into k subregions where the image intensity has a Gaussian distribution of mean c_i and of standard deviation σ_i. The second term is the regularization energy; minimizing it is equivalent to minimizing the interface between clusters. Minimizing the third term leads to a solution where the formation of a vacuum (pixel with no labels) and overlapping (pixel with more than one labels) regions are penalized.

As the first attempt of data clustering manipulated by the use of variational method, Samson's model has an advantage over the traditional clustering algorithms in obtaining the smooth cluster boundaries and the closed cluster regions. However, there are still some drawbacks as follows.

(1) Samson's model is actually a hard C means clustering which lacks the ability to retain abundant information from the original image and is also very sensitive to noise.

(2) The external clustering energy (the first term of $E(\phi_1 \cdots \phi_k)$) is point-based, which makes the clustering results sensitive to noise and outliers.

(3) It is a supervised image classification model. The cluster number k and the cluster centers $\{c_i\}_{i=1}^k$ must be given by the preclustering. In addition, the updating schemes for the cluster centers are not introduced by Samson et al. So, the clustering result is very sensitive to the choice of the initial cluster centers.

(4) The evolving level set function $\phi_i(\mathbf{x}, t)$ needs periodical reinitialization to keep it close to a signed distance function during its evolution by solving the following PDE:

$$\frac{\partial \phi_i(\mathbf{x}, t)}{\partial t} = \operatorname{sign}(\phi_i(\mathbf{x}, t)) \left(1 - \left|\nabla \phi_i(\mathbf{x}, t)\right|\right). \tag{7}$$

In this paper, following Samson's work, we propose a variational level set model combined with FCMS clustering (VFCMS) for image clustering segmentation. Four schemes are introduced to resolve the above mentioned drawbacks of Samson's model (6).

(1) A block-based clustering energy and a spatial constraint are introduced into the energy functional. In addition, the fuzziness of belongingness of each pixel to the cluster centers is introduced. These improvements enable the new model to be more robust to noises than Samson's model and FCMS clustering.

(2) A variational formulation is proposed for updating membership functions and cluster centers, which makes the new model more robust to the initial cluster centers and achieves a semisupervised clustering.

(3) A regularization term based on a new edge stopping function is proposed, which enables the active contours to move quickly through the noise regions and reach the right boundaries of image.

(4) A regularization term is introduced to eliminate the need of the costly reinitialization procedure.

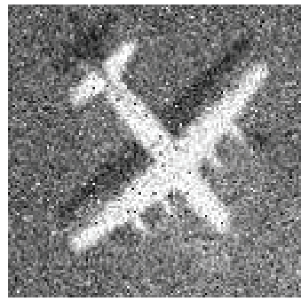

(a) Noisy data

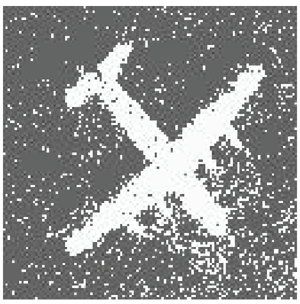

(b) FCM

(c) $FCMS_1$

(d) $FCMS_2$

(e) GFCMS

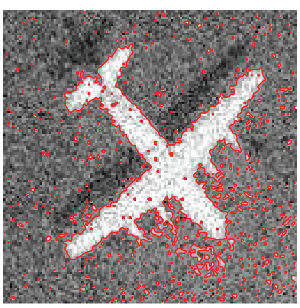

(f) CV (ZLSs)

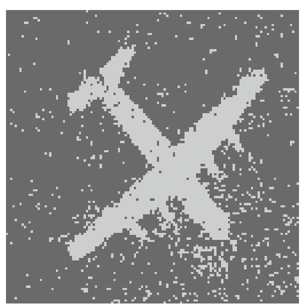

(g) CV

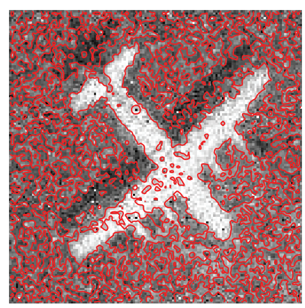

(h) LIF (ZLSs)

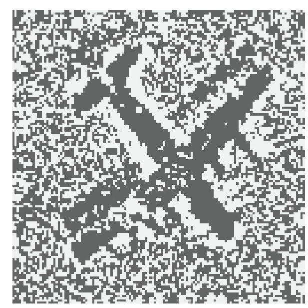

(i) LIF

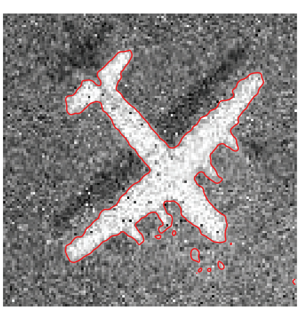

(j) RBACM (ZLSs)

(k) RBACM

(l) Samson's model (ZLSs)

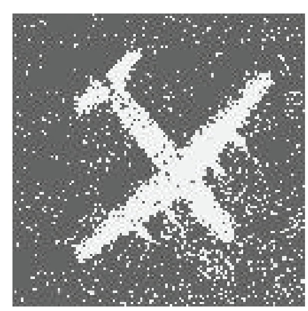

(m) Samson's model

(n) $VFCMS_1$ (ZLSs)

(o) $VFCMS_1$

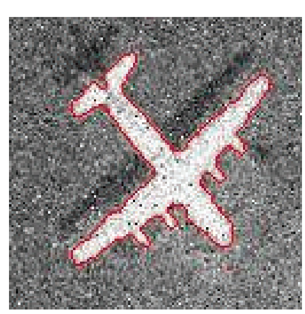

(p) $VFCMS_2$ (ZLSs)

(q) $VFCMS_2$

Figure 6: Continued.

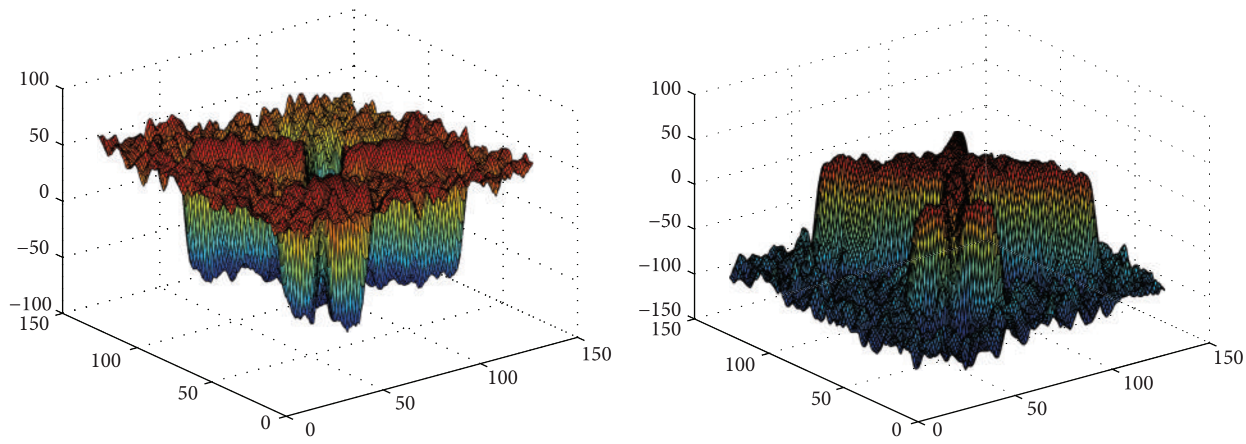

(r) The surface plot of ϕ_1

(s) The surface plot of ϕ_2

Figure 6: Comparison of segmentation results on a plane image with mixed 2% Salt and Pepper, Gaussian, and Speckle noise (cluster number $k = 2$).

3. The Proposed VFCMS Model

3.1. External Energy

3.1.1. Fuzzy Clustering Energy. The external clustering energy proposed by Samson et al. in [21] is defined as

$$\sum_{i=1}^{k} e_i \int_\Omega \frac{(f(\mathbf{x}) - c_i)^2}{\sigma_i} H(\phi_i(\mathbf{x}))\, d\mathbf{x} = \sum_{i=1}^{k} \int_\Omega \frac{e_i}{\sigma_i} (f(\mathbf{x}) - c_i)^2 H(\phi_i(\mathbf{x}))\, d\mathbf{x}. \tag{8}$$

Unfortunately, minimizing directly this energy functional to achieve the image clustering has two drawbacks: (1) it is sensitive to noises since it is point-based and (2) the ratio e_i/σ_i of weighted parameter e_i to the standard deviation σ_i can be seen as the membership between the image pixel $f(\mathbf{x})$ and the cluster center c_i. In [21], these two parameters are both chosen as constants. So, the clustering algorithm proposed by Samson et al. in [21] is actually a hard C means clustering. To deal with the first problem, (1) the use of block-based energy and (2) incorporating spatial information into the energy are appropriate choices. For the second problem, fuzziness of the belongingness of each image pixel should be incorporated into the clustering energy. Most existing fuzzy clustering algorithms are based on the discrete data and utilize the membership matrix to determine the belongingness of each data. The matrix is difficult to incorporate into the variational formulation directly. In this paper, we introduce continuous membership function $\mu_i(\mathbf{x})$ which can be easily manipulated in the variational problem.

Based on the points discussed above, we introduce the following fuzzy and block-based clustering energy:

$$\begin{gathered} \mathscr{E}_1^A(\phi_1 \cdots \phi_k, \mu_i, c_i) \\ = \sum_{i=1}^{k} \int_\Omega \mu_i^m(\mathbf{x}) \int_\Omega G_\sigma(\mathbf{x}-\mathbf{y}) (f(\mathbf{y}) - c_i)^2 d\mathbf{y} H(\phi_i(\mathbf{x}))\, d\mathbf{x}, \\ \text{s.t. } \sum_{i=1}^{k} H(\phi_i(\mathbf{x})) = 1, \quad \sum_{i=1}^{k} \mu_i(\mathbf{x}) = 1, \end{gathered} \tag{9}$$

where $G_\sigma(\mathbf{x})$ is a point spread function, (e.g., Gaussian function with standard deviation σ). The constraint $\sum_{i=1}^{k} H(\phi_i(\mathbf{x})) = 1$ is to penalize the overlapping and vacuum formation of the clustering regions and $\sum_{i=1}^{k} \mu_i(\mathbf{x}) = 1$ is a nature constraint.

In what follows, we analyze this energy in the theory. Denote

$$\tilde{f}(\mathbf{x}) = \int_\Omega G_\sigma(\mathbf{x}-\mathbf{y}) f(\mathbf{y})\, d\mathbf{y} = (G_\sigma * f)(\mathbf{x}). \tag{10}$$

The point spread function $G_\sigma(\mathbf{x})$ satisfies that $\int G_\sigma(\mathbf{x}) d\mathbf{x} = 1$. Thus we have

$$\begin{aligned} &\int_\Omega G_\sigma(\mathbf{x}-\mathbf{y}) (f(\mathbf{y}) - c_i)^2 d\mathbf{y} \\ &\quad = \int_\Omega G_\sigma(\mathbf{x}-\mathbf{y}) \left(f(\mathbf{y}) - \tilde{f}(\mathbf{x}) + \tilde{f}(\mathbf{x}) - c_i\right)^2 d\mathbf{y} \\ &\quad = \int_\Omega G_\sigma(\mathbf{x}-\mathbf{y}) \left(f(\mathbf{y}) - \tilde{f}(\mathbf{x})\right)^2 d\mathbf{y} \\ &\qquad + \left(\tilde{f}(\mathbf{x}) - c_i\right)^2 \int_\Omega G_\sigma(\mathbf{x}-\mathbf{y})\, d\mathbf{y} \\ &\qquad + 2 \int_\Omega G_\sigma(\mathbf{x}-\mathbf{y}) \left(f(\mathbf{y}) - \tilde{f}(\mathbf{x})\right) \left(\tilde{f}(\mathbf{x}) - c_i\right) d\mathbf{y} \\ &\quad = \int_\Omega G_\sigma(\mathbf{x}-\mathbf{y}) \left(f(\mathbf{y}) - \tilde{f}(\mathbf{x})\right)^2 d\mathbf{y} + \left(\tilde{f}(\mathbf{x}) - c_i\right)^2 \\ &\qquad + 2 \int_\Omega G_\sigma(\mathbf{x}-\mathbf{y}) \left(f(\mathbf{y}) - \tilde{f}(\mathbf{x})\right) \left(\tilde{f}(\mathbf{x}) - c_i\right) d\mathbf{y} \end{aligned} \tag{11}$$

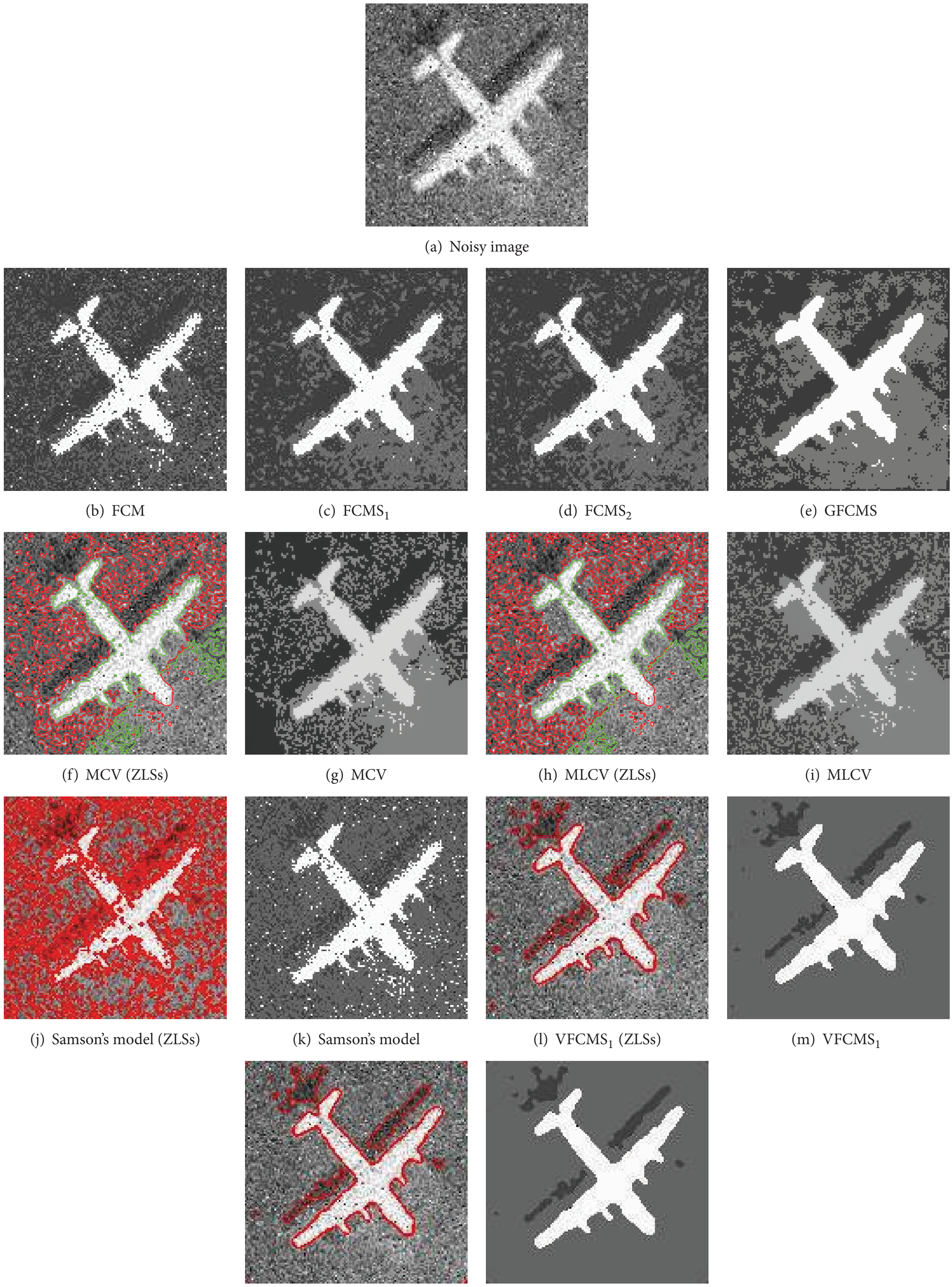

(a) Noisy image

(b) FCM

(c) FCMS_1

(d) FCMS_2

(e) GFCMS

(f) MCV (ZLSs)

(g) MCV

(h) MLCV (ZLSs)

(i) MLCV

(j) Samson's model (ZLSs)

(k) Samson's model

(l) VFCMS_1 (ZLSs)

(m) VFCMS_1

(n) VFCMS_2 (ZLSs)

(o) VFCMS_2

Figure 7: Continued.

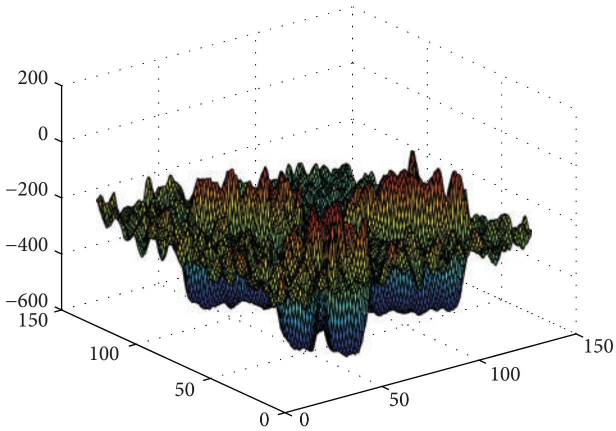

(p) The surface plot of ϕ_1

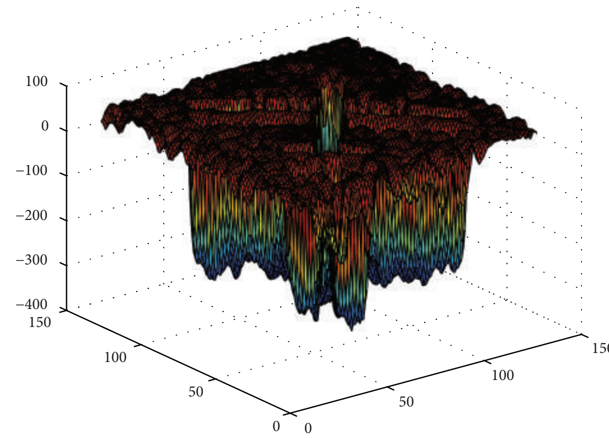

(q) The surface plot of ϕ_2

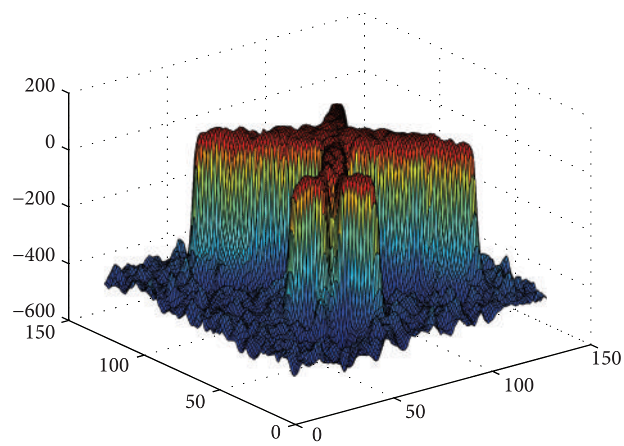

(r) The surface plot of ϕ_3

Figure 7: Comparison of segmentation results on a plane image with mixed 2% Salt and Pepper, Gaussian, and Speckle noise (cluster number $k = 3$).

in which

$$\begin{aligned}
&\int_\Omega G_\sigma(\mathbf{x}-\mathbf{y})\left(f(\mathbf{y})-\tilde{f}(\mathbf{x})\right)\left(\tilde{f}(\mathbf{x})-c_i\right)d\mathbf{y} \\
&\quad=\left(\tilde{f}(\mathbf{x})-c_i\right)\int_\Omega G_\sigma(\mathbf{x}-\mathbf{y})\,f(\mathbf{y})\,d\mathbf{y} \\
&\qquad-\tilde{f}(\mathbf{x})\left(\tilde{f}(\mathbf{x})-c_i\right)\int_\Omega G_\sigma(\mathbf{x}-\mathbf{y})\,d\mathbf{y} \\
&\quad=\left(\tilde{f}(\mathbf{x})-c_i\right)\tilde{f}(\mathbf{x})-\tilde{f}(\mathbf{x})\left(\tilde{f}(\mathbf{x})-c_i\right)=0, \\
&\int_\Omega G_\sigma(\mathbf{x}-\mathbf{y})\left(f(\mathbf{y})-\tilde{f}(\mathbf{x})\right)^2 d\mathbf{y} \\
&\quad=\int_\Omega G_\sigma(\mathbf{x}-\mathbf{y})\,(f(\mathbf{y}))^2 d\mathbf{y}+\int_\Omega G_\sigma(\mathbf{x}-\mathbf{y})\left(\tilde{f}(\mathbf{x})\right)^2 d\mathbf{y} \\
&\qquad-2\int_\Omega G_\sigma(\mathbf{x}-\mathbf{y})\,f(\mathbf{y})\,\tilde{f}(\mathbf{x})\,d\mathbf{y} \\
&\quad=\int_\Omega G_\sigma(\mathbf{x}-\mathbf{y})\,(f(\mathbf{y}))^2 d\mathbf{y}-\left(\tilde{f}(\mathbf{x})\right)^2.
\end{aligned} \tag{12}$$

From the last equation, we have

$$\int_\Omega G_\sigma(\mathbf{x}-\mathbf{y})\,(f(\mathbf{y}))^2 d\mathbf{y}-\left(\tilde{f}(\mathbf{x})\right)^2 \longrightarrow 0 \quad \text{as } \sigma \longrightarrow 0. \tag{13}$$

If we ignore this term, the energy functional (9) can be rewritten as

$$\begin{aligned}
&\mathscr{E}_1^A(\phi_1\cdots\phi_k,\mu_i,c_i) \\
&\quad=\sum_{i=1}^k\int_\Omega \mu_i^m(\mathbf{x})\left(\tilde{f}(\mathbf{x})-c_i\right)^2 H(\phi_i(\mathbf{x}))\,d\mathbf{x}, \\
&\text{s.t.}\ \sum_{i=1}^k H(\phi_i(\mathbf{x}))=1,\qquad \sum_{i=1}^k \mu_i(\mathbf{x})=1.
\end{aligned} \tag{14}$$

Since $\tilde{f}(\mathbf{x})$ can be seen as a denoised image with a smoothing kernel $G_\sigma(\mathbf{x})$, minimizing energy (14) is equivalent to cluster the denoised image by FCM clustering. Thus, the proposed model is more robust to noise than the standard FCM clustering and Samson's model.

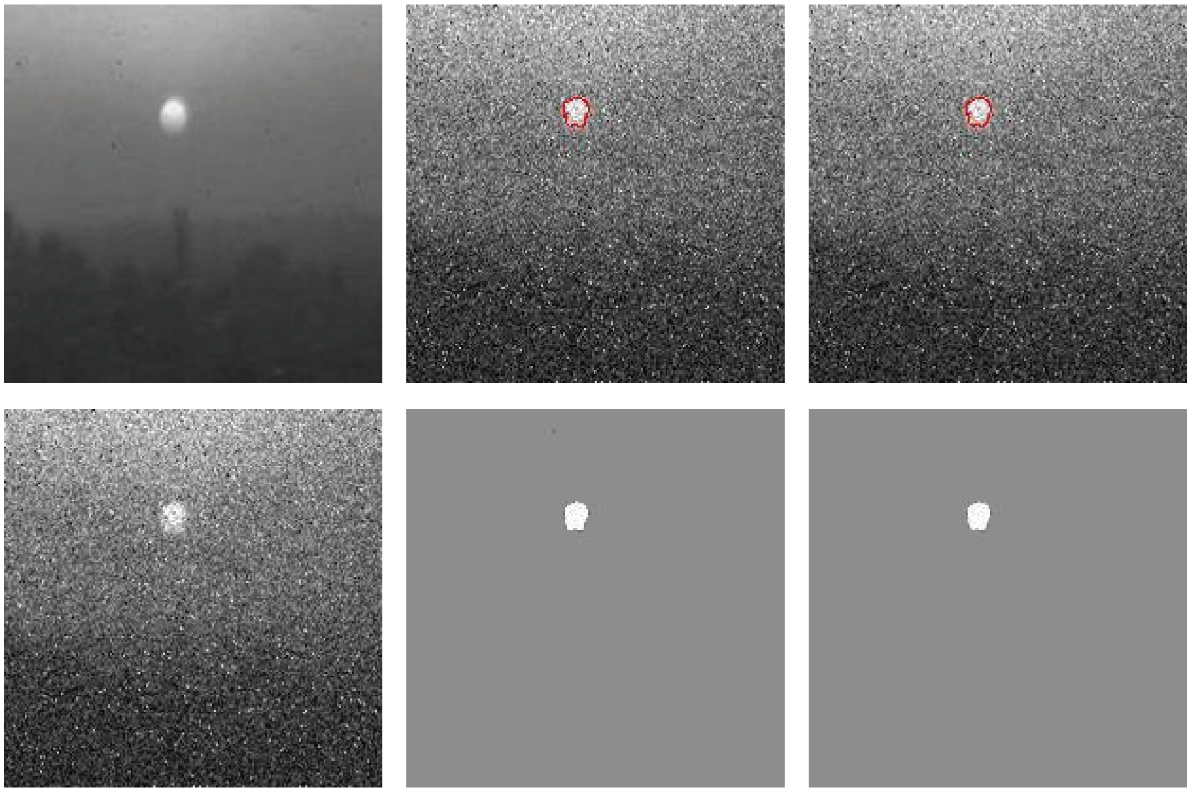

(a) Original image and its noisy version (b) VFCMS_1 (c) VFCMS_2

Figure 8: Segmentation results on a sun image with mixed 2% Salt and Pepper, Gaussian, and Speckle noise (cluster number $k = 2$).

In order to further increase the robustness to noises, we introduce the following spatial constraint into the energy functional. Note that here we adopt a modified form proposed by Chen and Zhang in [16] to save the computing time.

$$\mathscr{E}_2^A(\phi_1\cdots\phi_k,\mu_i,c_i) = \sum_{i=1}^{k}\alpha\int_\Omega \mu_i^m(\mathbf{x})\left(\overline{f}(\mathbf{x})-c_i\right)^2 H(\phi_i(\mathbf{x}))\,d\mathbf{x}, \quad \text{s.t. } \sum_{i=1}^{k}H(\phi_i(\mathbf{x}))=1, \quad \sum_{i=1}^{k}\mu_i(\mathbf{x})=1, \tag{15}$$

where $\alpha > 0$ is a tuning parameter and $\overline{f}(\mathbf{x})$ can be can be considered to be the mean or median of $f(\mathbf{x})$ supported on the disk centered at $\mathbf{x}$. Similar to (4), the value of $\overline{f}(\mathbf{x})$ can be computed in advance, thus the clustering time can be saved.

Combining (9) and (15), the total external clustering energy is

$$\begin{aligned}\mathscr{E}^A(\phi_1\cdots\phi_k,\mu_i,c_i) &= \mathscr{E}_1^A(\phi_1\cdots\phi_k,\mu_i,c_i)+\mathscr{E}_2^A(\phi_1\cdots\phi_k,\mu_i,c_i)\\ &= \sum_{i=1}^{k}\int_\Omega \mu_i^m(\mathbf{x})\int_\Omega G_\sigma(\mathbf{x}-\mathbf{y})(f(\mathbf{y})-c_i)^2 d\mathbf{y}H(\phi_i(\mathbf{x}))\,d\mathbf{x}\\ &\quad+\sum_{i=1}^{k}\alpha\int_\Omega \mu_i^m(\mathbf{x})\left(\overline{f}(\mathbf{x})-c_i\right)^2 H(\phi_i(\mathbf{x}))\,d\mathbf{x},\\ \text{s.t. } &\sum_{i=1}^{k}H(\phi_i(\mathbf{x}))=1, \quad \sum_{i=1}^{k}\mu_i(\mathbf{x})=1.\end{aligned} \tag{16}$$

Similar to [16], for convenience of notation later, the proposed VFCMS model is renamed as VFCMS_1 and VFCMS_2 corresponding to $\overline{f}(\mathbf{x})$ being median filtering and mean filtering, respectively. In addition, in what follows, we always write

$$\int_\Omega G_\sigma(\mathbf{x}-\mathbf{y})(f(\mathbf{y})-c_i)^2 d\mathbf{y} = \left(G_\sigma * (f-c_i)^2\right)(\mathbf{x}). \tag{17}$$

3.1.2. The Optimal Membership Functions. Fixing level set functions $\{\phi_i\}_{i=1}^k$ and clustering centers $\{c_i\}_{i=1}^k$, we seek the optimal membership functions $\mu_i(\mathbf{x})$ which make the energy functional $\mathscr{E}^A(\phi_1\cdots\phi_k,\mu_i,c_i)$ to converge to a local minimum. In order to improve the ability of active contour to capture the pixels belonging to its cluster, we compute the optimal membership functions that are supported on the whole image domain Ω, that is, computing the membership relations between each pixel $\mathbf{x}$ and each cluster center c_i. Firstly, we extend the fuzzy clustering energy $\mathscr{E}^A(\phi_1\cdots\phi_k,\mu_i,c_i)$ to the whole image domain Ω, denoted as $\mathscr{E}_\Omega^A(\phi_1\cdots\phi_k,\mu_i,c_i)$. Minimizing $\mathscr{E}_\Omega^A(\phi_1\cdots\phi_k,\mu_i,c_i)$ with

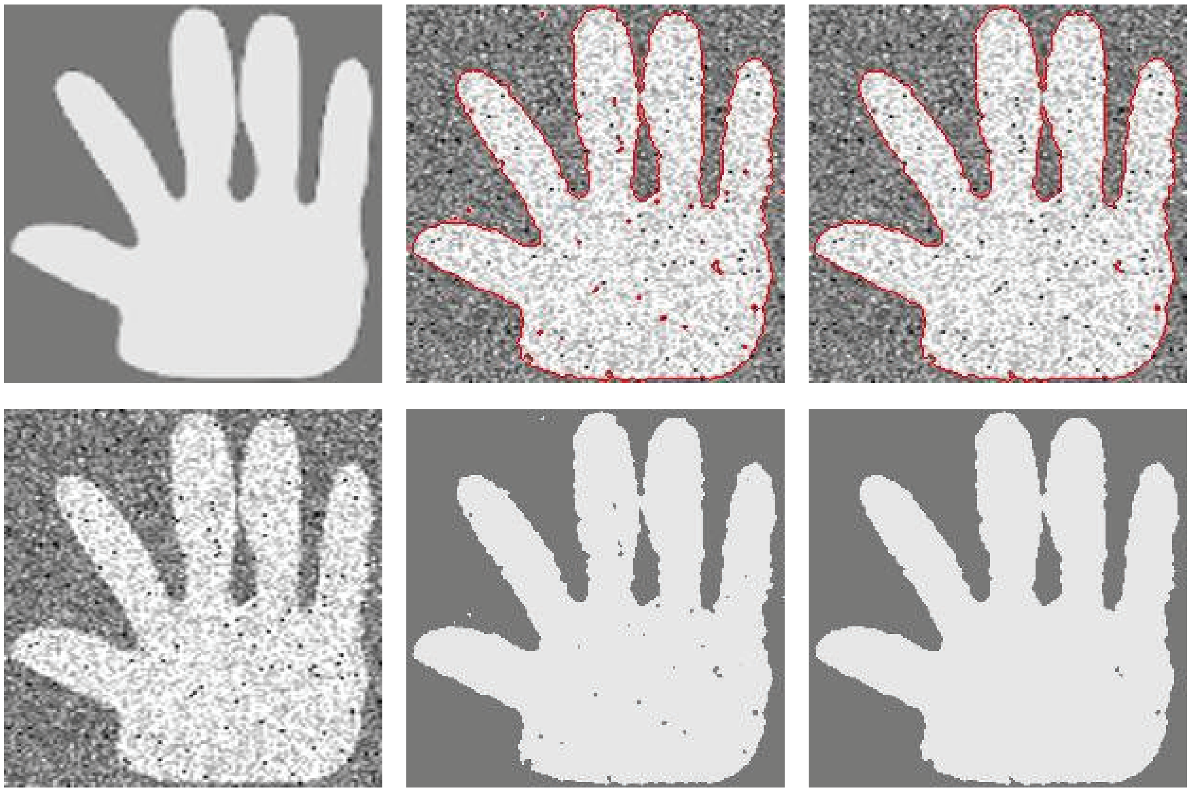

(a) Original image and its noisy version (b) VFCMS$_1$ (c) VFCMS$_2$

Figure 9: Segmentation results on a palm image with mixed 2% Salt and Pepper, Gaussian, and Speckle noise (cluster number $k = 2$).

respect to each $\mu_i(\mathbf{x})$, we can obtain the optimal membership functions supported on total image domain Ω. The detail is stated as follows:

$$\min_{\mu_i(\mathbf{x})} \left\{ \mathscr{E}_\Omega^A(\phi_1 \cdots \phi_k, \mu_i, c_i) = \sum_{i=1}^{k} \int_\Omega \mu_i^m(\mathbf{x}) \left(G_\sigma * (f - c_i)^2\right)(\mathbf{x})\, d\mathbf{x} + \sum_{i=1}^{k} \alpha \int_\Omega \mu_i^m(\mathbf{x}) \left(\overline{f}(\mathbf{x}) - c_i\right)^2 d\mathbf{x} \right\}, \quad \text{s.t.} \sum_{i=1}^{k} \mu_i(\mathbf{x}) = 1. \tag{18}$$

Using calculus of variation and Lagrange multiplier method, the necessary condition on $\mu_i(\mathbf{x})$ for (18) to be at a local minimum is

$$\begin{aligned}\mu_1^{m-1}(\mathbf{x}) \left(G_\sigma * (f - c_i)^2\right)(\mathbf{x}) + \alpha\mu_1^{m-1}(\mathbf{x}) \left(\overline{f}(\mathbf{x}) - c_i\right)^2 &= \cdots = \mu_k^{m-1}(\mathbf{x}) \left(G_\sigma * (f - c_i)^2\right)(\mathbf{x}) + \alpha\mu_k^{m-1}(\mathbf{x}) \left(\overline{f}(\mathbf{x}) - c_i\right)^2, \\ \sum_{i=1}^{k} \mu_i(\mathbf{x}) &= 1.\end{aligned} \tag{19}$$

Solving each $\mu_i(\mathbf{x})$ in the last equations, we can obtain the optimal membership functions

$$\mu_i(\mathbf{x}) = \frac{\left(\left(G_\sigma * (f - c_i)^2\right)(\mathbf{x}) + \alpha\left(\overline{f}(\mathbf{x}) - c_i\right)^2\right)^{-1/(m-1)}}{\sum_{t=1}^{k} \left(\left(G_\sigma * (f - c_i)^2\right)(\mathbf{x}) + \alpha\left(\overline{f}(\mathbf{x}) - c_t\right)^2\right)^{-1/(m-1)}}. \tag{20}$$

In the experiments, (20) gives us the updating formula of the optimal membership functions.

3.1.3. The Optimal Cluster Centers. Fixing level set functions $\{\phi_i\}_{i=1}^k$ and membership functions $\{\mu_i\}_{i=1}^k$, we seek the optimal cluster centers $\{c_i\}_{i=1}^k$ which make the energy functional $\mathscr{E}^A(\phi_1 \cdots \phi_k, \mu_i, c_i)$ to be a local minimum. That is, minimizing the energy

$$\sum_{i=1}^{k} \int_\Omega \mu_i^m(\mathbf{x}) \left(G_\sigma * (f - c_i)^2\right)(\mathbf{x})\, H(\phi_i(\mathbf{x}))\, d\mathbf{x} + \sum_{i=1}^{k} \alpha \int_\Omega \mu_i^m(\mathbf{x}) \left(\overline{f}(\mathbf{x}) - c_i\right)^2 H(\phi_i(\mathbf{x}))\, d\mathbf{x} \tag{21}$$

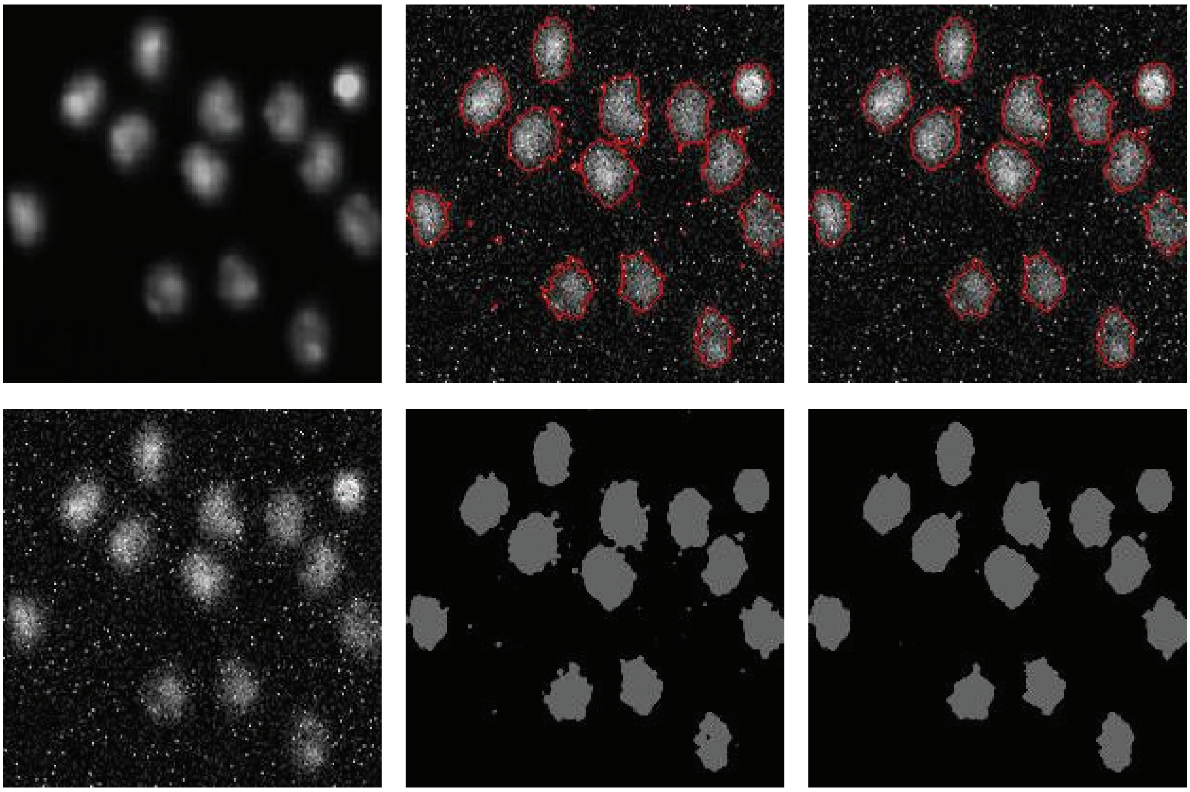

(a) Original image and its noisy version (b) VFCMS_1 (c) VFCMS_2

FIGURE 10: Segmentation results on a light image with mixed 2% Salt and Pepper, Gaussian, and Speckle noise (cluster number $k = 2$).

with respect to each c_i. The necessary condition on c_i for (21) to be a local minimum is

$$\sum_{i=1}^{k}\int_{\Omega}\mu_i^m(\mathbf{x})\left(G_\sigma*(f-c_i)\right)(\mathbf{x})\,H\left(\phi_i(\mathbf{x})\right)d\mathbf{x} + \sum_{i=1}^{k}\alpha\int_{\Omega}\mu_i^m(\mathbf{x})\left(\overline{f}(\mathbf{x})-c_i\right)H\left(\phi_i(\mathbf{x})\right)d\mathbf{x}=0. \tag{22}$$

Solving c_i in the last equation, we have

$$c_i=\frac{\int_{\Omega}\mu_i^m(\mathbf{x})\left(\left(G_\sigma*f\right)(\mathbf{x})+\alpha\overline{f}(\mathbf{x})\right)H\left(\phi_i(\mathbf{x})\right)d\mathbf{x}}{(1+\alpha)\int_{\Omega}\mu_i^m(\mathbf{x})\,H\left(\phi_i(\mathbf{x})\right)d\mathbf{x}}. \tag{23}$$

The optimal cluster center c_i is actually the weighted mean of $f(\mathbf{x})$ supported on the Ω_i. Equation (23) gives us the updating formula of the optimal cluster centers in the iterative process.

3.2. The Internal Energy. In this section, we introduce two internal energies $\mathscr{E}_1^B$ and $\mathscr{E}_2^B$, where $\mathscr{E}_1^B$ is to penalize the singularities of level set functions and $\mathscr{E}_2^B$ is to penalize the formation of vacuum and overlapping regions.

In the traditional variational level set method for image processing, in order to maintain the stability of the level set function during the evolution, the evolving level set function needs periodical reinitialization to keep it close to a signed distance function [22]. Samson et al. achieved the reinitialization by periodically solving PDEs (7). Many serious problems remain such as when to apply the reinitialization and the computational complexity increases. In this paper, we adopt method proposed by Zhang et al. in [23] and introduce the following internal energy:

$$\mathscr{E}_1^B\left(\phi_1\cdots\phi_k\right)=\frac{1}{2}\sum_{i=1}^{k}\lambda\int_{\Omega}\left|\nabla\phi_i(\mathbf{x})\right|^2d\mathbf{x} \tag{24}$$

to eliminate the need of the expensive reinitialization procedure. Here, $\lambda > 0$ is a tuning parameter. The energy $\mathscr{E}_1^B$ can be identified as a metric to measure the smoothness of the level set function.

The constraint $\sum_{i=1}^{k} H(\phi_i(\mathbf{x})) = 1$ is to penalize the vacuum and overlapping regions. In this paper, similar to (6), we introduce the following internal energy to meet this constraint:

$$\mathscr{E}_2^B\left(\phi_1\cdots\phi_k\right)=\frac{1}{2}\kappa\int_{\Omega}\left(\sum_{i=1}^{k}H\left(\phi_i(\mathbf{x})\right)-1\right)^2d\mathbf{x}, \tag{25}$$

where $\kappa > 0$ is a tuning parameter. The value of $\sum_{i=1}^{k} H(\phi_i(\mathbf{x}))$ will trend to 1 in the process of minimizing the energy $\mathscr{E}_2^B$. So, the overlapping and vacuum cluster regions will decrease in

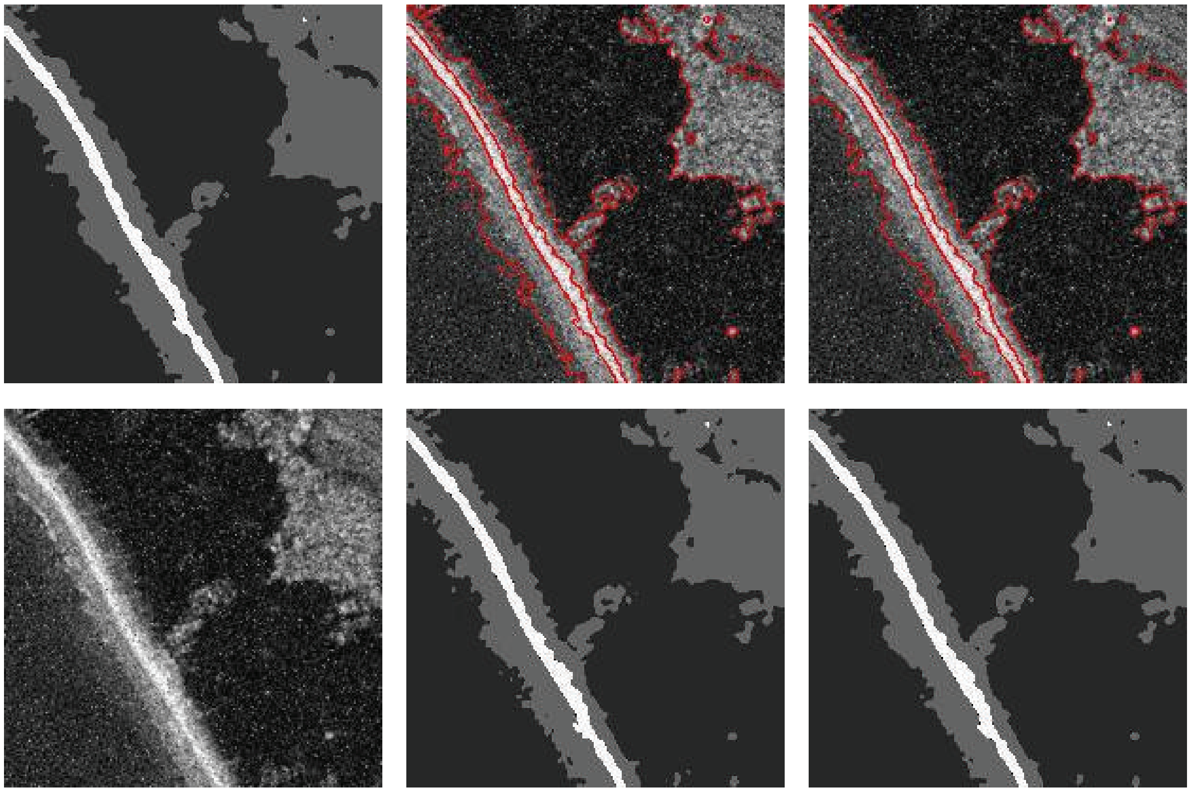

(a) Original image and its noisy version (b) VFCMS$_1$ (c) VFCMS$_2$

Figure 11: Segmentation results on satellite image with mixed 2% Salt and Pepper, Gaussian, and Speckle noise (cluster number $k = 3$).

the process of clustering. In what follows, we write the total of internal energy as

$$\mathscr{E}^B(\phi_1\cdots\phi_k) = \mathscr{E}_1^B(\phi_1\cdots\phi_k) + \mathscr{E}_2^B(\phi_1\cdots\phi_k). \quad (26)$$

3.3. The Regularization Energy. Samson et al. [21] introduced the following regularization energy to smooth the boundaries of the clusters:

$$\begin{aligned}\mathscr{E}^C(\phi_1\cdots\phi_k) &= \sum_{i=1}^{k}\gamma\int_{\phi_i=0} ds \\ &= \sum_{i=1}^{k}\gamma\int_{\Omega} g(f(\mathbf{x}))\left|\nabla H(\phi_i(\mathbf{x}))\right| d\mathbf{x},\end{aligned} \quad (27)$$

where the stopping function is defined as

$$g(f(\mathbf{x})) = \frac{1}{1+\left|\nabla G_\sigma * f(\mathbf{x})\right|^2}, \quad (28)$$

which is a decreasing function of the gradient module of image. The evolving velocity of ZLS is about one ($g(f(\mathbf{x})) \to 1$) at the smooth position of the image, since the gradient module is about zero ($|\nabla f(\mathbf{x})| \to 0$) at this position, which makes the ZLS to move quickly through the smooth position. At the position of the edge, the gradient module $|\nabla f(\mathbf{x})| \to \infty$ and the evolving velocity $g(f(\mathbf{x})) \to 0$, which makes the ZLS to stay the edges. But if the data is very noisy, the evolving velocity of ZLS is about zero at the position of isolated noise, since the gradient module is about infinite at this position, which makes ZLS stay at the position of isolated noise and results in failed image segmentation. So, the traditional edge indicators based on the image gradient module cannot effectively distinguish between edges and isolated noises. In [24], the authors presented a new edge indicator based on the second derivatives, which is defined as

$$D = \left|\left|f_{\eta\eta}\right| - \left|f_{\xi\xi}\right|\right|, \quad (29)$$

where $f_{\eta\eta}$ and $f_{\xi\xi}$ represent the second directional derivatives in the direction of the gradient ∇f and in the perpendicular direction of ∇f, respectively. $|\cdot|$ denotes the absolute value. The performance of the new edge indicator is as follows: (1) for the edges, $|f_{\eta\eta}|$ is large and $|f_{\xi\xi}|$ is small, so D is large and (2) for the isolated noises, $|f_{\eta\eta}|$ and $|f_{\xi\xi}|$ are both large and almost equal, so D is small. According to the analysis mentioned above, edges and isolated noises can be well distinguished based on the value of D.

In this paper, we use a new stopping function in regularization energy (27)

$$g(f(\mathbf{x})) = \frac{1}{1+\left|D(G_\sigma * f(\mathbf{x}))\right|^2}, \quad (30)$$

which is based on the edge indicator (29).

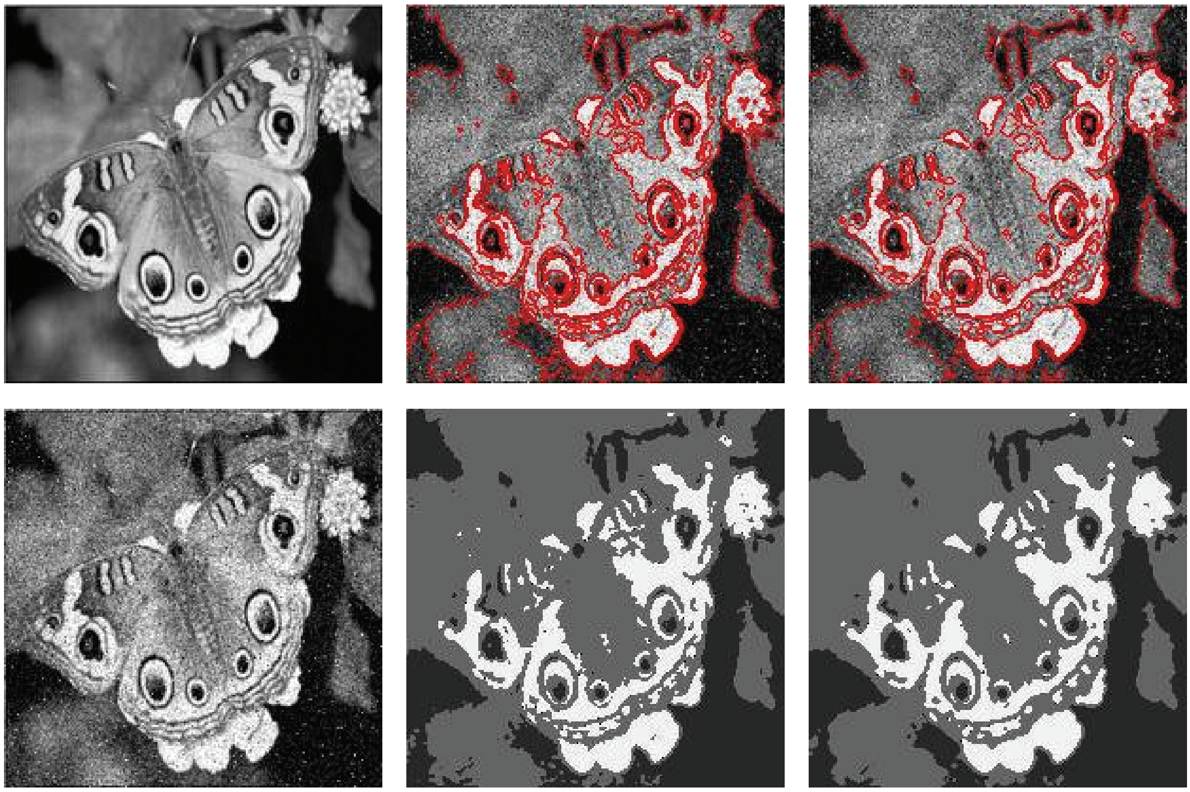

(a) Original image and its noisy version (b) VFCMS_1 (c) VFCMS_2

FIGURE 12: Segmentation results on a butterfly image with mixed 2% Salt and Pepper, Gaussian, and Speckle noise (cluster number $k = 3$).

3.4. The Numerical Implementation. Combined with external energy $\mathscr{E}^A$, internal energy $\mathscr{E}^B$ and regularization energy $\mathscr{E}^C$, image clustering segmentation is equivalent to minimize the following energy functional:

$$\begin{aligned}\mathscr{E}(\phi_1\cdots\phi_k,\mu_i,c_i) &= \mathscr{E}^A(\phi_1\cdots\phi_k,\mu_i,c_i)+\mathscr{E}^B(\phi_1\cdots\phi_k)+\mathscr{E}^C(\phi_1\cdots\phi_k)\\ &= \frac{1}{2}\sum_{i=1}^{k}\lambda\int_\Omega|\nabla\phi_i(\mathbf{x})|^2d\mathbf{x}+\frac{1}{2}\kappa\int_\Omega\left(\sum_{i=1}^{k}H(\phi_i(\mathbf{x}))-1\right)^2d\mathbf{x}\\ &\quad+\sum_{i=1}^{k}\int_\Omega\mu_i^m(\mathbf{x})\left(G_\sigma*(f-c_i)^2\right)(\mathbf{x})H(\phi_i(\mathbf{x}))d\mathbf{x}\\ &\quad+\sum_{i=1}^{k}\alpha\int_\Omega\mu_i^m(\mathbf{x})\left(\overline{f}(\mathbf{x})-c_i\right)^2H(\phi_i(\mathbf{x}))d\mathbf{x}\\ &\quad+\sum_{i=1}^{k}\gamma\int_\Omega g(f(\mathbf{x}))|\nabla H(\phi_i(\mathbf{x}))|d\mathbf{x}.\end{aligned}\tag{31}$$

In experiments, we choose $G_\sigma(\mathbf{x})$ Gaussian function with standard deviation σ, that is,

$$G_\sigma(\mathbf{x})=\frac{1}{2\pi\sigma}\exp\left(-\frac{|\mathbf{x}|^2}{2\sigma^2}\right).\tag{32}$$

The functional $\mathscr{E}$ still has a drawback from the practical point of view; that is, $\mathscr{E}$ is not Gateaux differentiable. So we have to regularize $\mathscr{E}$. To do this, we use the following regularization Heaviside and Dirac function defined as

$$\begin{aligned}H_\varepsilon(s)&=\begin{cases}\dfrac{1}{2}\left(1+\dfrac{s}{\varepsilon}+\dfrac{1}{\pi}\sin\left(\dfrac{\pi s}{\varepsilon}\right)\right) & |s|\le\varepsilon\\ 1 & s>\varepsilon\\ 0 & s<-\varepsilon,\end{cases}\\ \delta_\varepsilon(s)&=\begin{cases}\dfrac{1}{2\varepsilon}\left(1+\cos\left(\dfrac{\pi s}{\varepsilon}\right)\right) & |s|<\varepsilon\\ 0 & s\ge\varepsilon\end{cases}\end{aligned}\tag{33}$$

to approximate the standard Heaviside and Dirac functions, respectively. In this paper, we choose that $\varepsilon = 5$.

Formally minimizing the energy (31) with respect to each ϕ_i yields the following K-coupled Euler-Lagrange equations:

$$\begin{aligned}-\lambda\Delta\phi_i+\delta_\varepsilon(\phi_i)\Bigg[&\mu_i^m(\mathbf{x})\left(G_\sigma*(f-c_i)^2\right)(\mathbf{x})\\ &+\alpha\mu_i^m(\mathbf{x})\left(\overline{f}(\mathbf{x})-c_i\right)^2\\ &-\gamma\,\mathrm{div}\left(g(f(\mathbf{x}))\frac{\nabla\phi_i}{|\nabla\phi_i|}\right)\\ &+\kappa\left(\sum_{i=1}^{k}H_\varepsilon(\phi_i(\mathbf{x}))-1\right)\Bigg]=0\end{aligned}\tag{34}$$

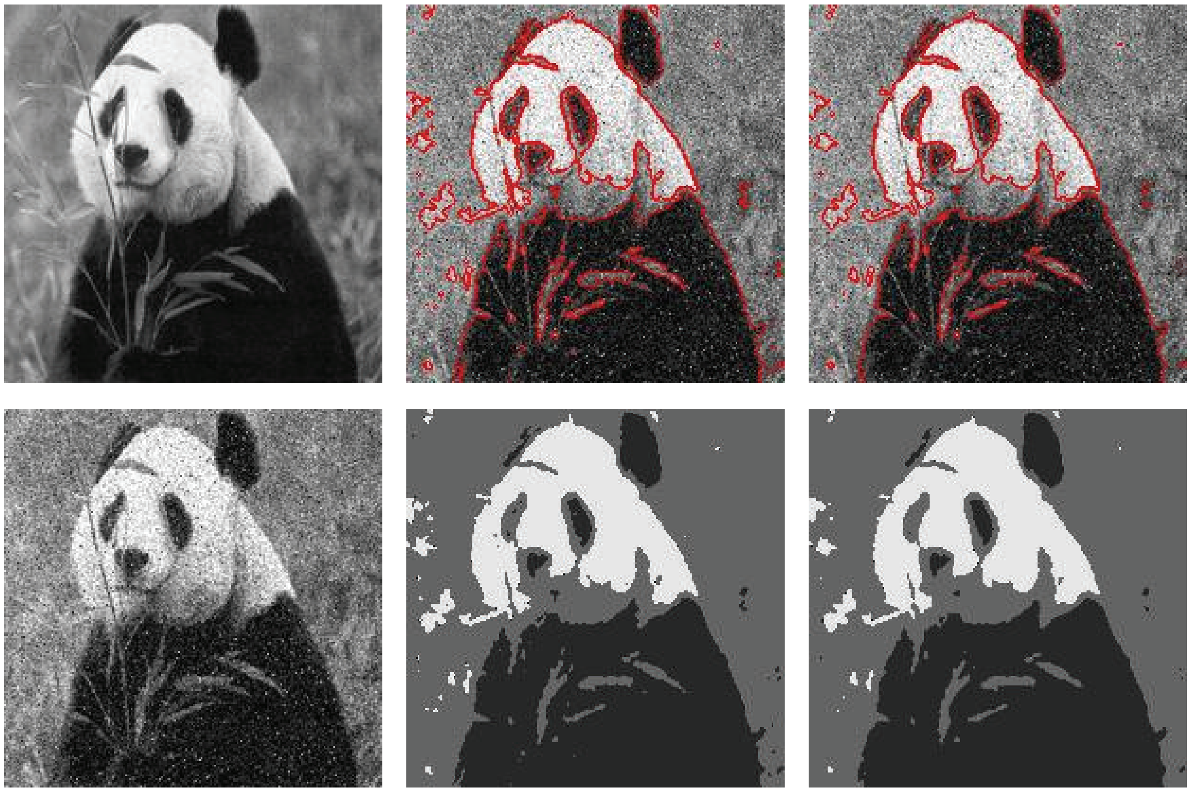

(a) Original image and its noisy version (b) VFCMS$_1$ (c) VFCMS$_2$

Figure 13: Segmentation results on a panda image with mixed 2% Salt and Pepper, Gaussian, and Speckle noise (cluster number $k = 3$).

for $i = 1, \ldots, k$, with the Neumann boundary conditions. To solve the K-coupled PDEs (34), adopting gradient descent scheme, we embed it into a dynamical process,

$$\begin{aligned}\frac{\partial \phi_i}{\partial t} &= \lambda \Delta \phi_i \\ &\quad - \delta_\varepsilon(\phi_i)\Bigg[\mu_i^m(\mathbf{x})\left(G_\sigma * (f - c_i)^2\right)(\mathbf{x}) \\ &\qquad + \alpha \mu_i^m(\mathbf{x})\left(\overline{f}(\mathbf{x}) - c_i\right)^2 \\ &\qquad - \gamma \operatorname{div}\left(g(f(\mathbf{x}))\frac{\nabla \phi_i}{|\nabla \phi_i|}\right) \\ &\qquad + \kappa\left(\sum_{i=1}^{k} H_\varepsilon(\phi_i(\mathbf{x})) - 1\right)\Bigg]\end{aligned} \tag{35}$$

with the initial conditions $\phi_i(x, y, 0) = \phi_{i,0}(x, y)$ for $i = 1, \ldots, k$. In this paper, we use the explicit finite difference scheme and two-step splitting method [23] to solve (35). The reader can refer to [23] for more details.

3.5. The Algorithm of Image Clustering Segmentation. Using updating formulas (20), (23), and (35) to update the membership functions $\{\mu_i(\mathbf{x})\}_{i=1}^k$, cluster centers $\{c_i\}_{i=1}^k$, and level set functions $\{\phi_i\}_{i=1}^k$ successively, we obtain the following iterative algorithm for VFCMS clustering segmentation model.

Algorithm (VFCMS Clustering)

Step 1. Given the number of the classes k and the initial level set functions $\{\phi_i\}_{i=1}^k$, choosing the initial cluster centers $\{c_i\}_{i=1}^k$.

Step 2. Fixed level set functions $\{\phi_i\}_{i=1}^k$ and cluster centers $\{c_i\}_{i=1}^k$, computing the optimal membership functions $\{\mu_i(\mathbf{x})\}_{i=1}^k$ by (20).

Step 3. Fixed cluster centers $\{c_i\}_{i=1}^k$ and membership functions $\{\mu_i(\mathbf{x})\}_{i=1}^k$, computing the optimal level set functions $\{\phi_i\}_{i=1}^k$ by solving the K-coupled PDEs (35).

Step 4. Fixed membership functions $\{\mu_i(\mathbf{x})\}_{i=1}^k$ and level set functions $\{\phi_i\}_{i=1}^k$, computing the optimal cluster centers $\{\overline{c}_i\}_{i=1}^k$ by (23).

Step 5. If $\max_i |\overline{c}_i - c_i| \le \varepsilon$, end the algorithm; else let $c_i = \overline{c}_i$ and go back to Step 2.

Step 6. Output the result of image clustering segmentation $u = \sum_{i=1}^k c_i H_\varepsilon(\phi_i(\mathbf{x}))$.

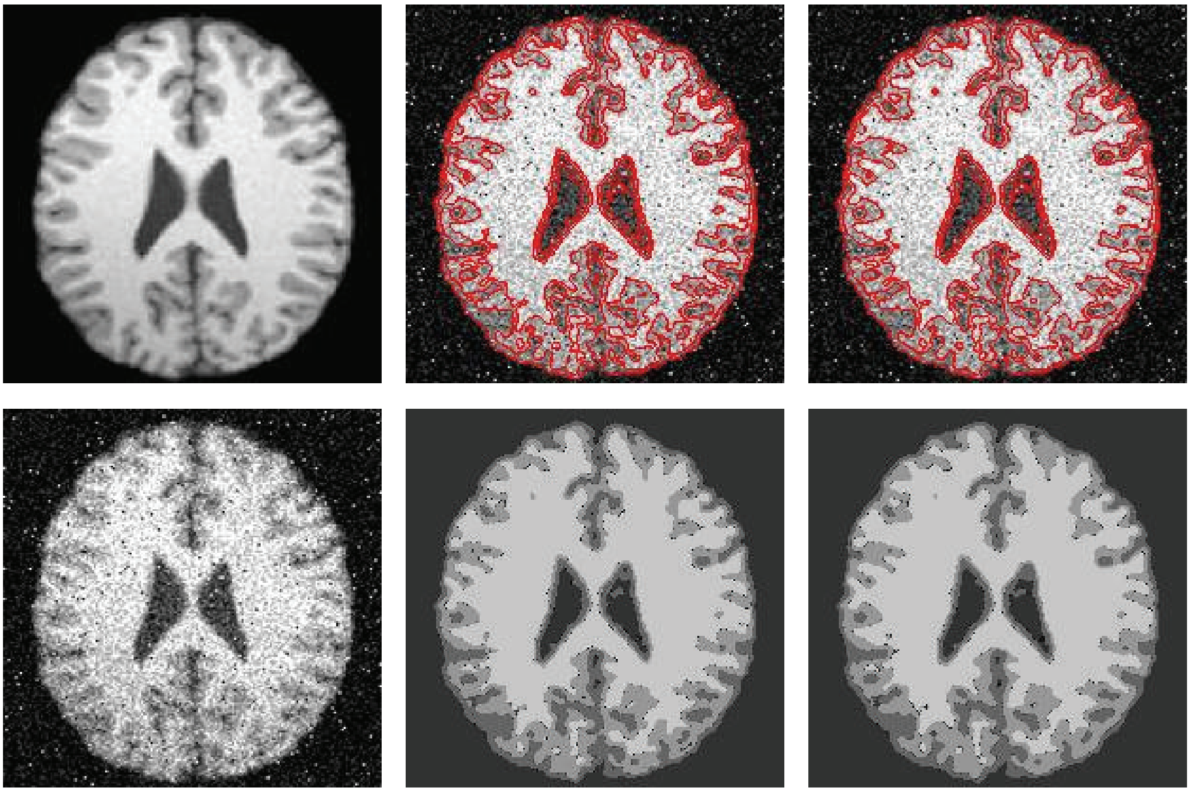

(a) Original image and its noisy version (b) VFCMS$_1$ (c) VFCMS$_2$

Figure 14: Segmentation results on a CT image with mixed 2% Salt and Pepper, Gaussian, and Speckle noise (cluster number $k = 4$).

4. Experimental Results

In this section, we show the experimental results of image segmentation on several synthetic and real images. There are a total of twelve models used in this section, that is, (1) clustering models (FCM, FCMS$_1$, FCMS$_2$, and GFCMS), (2) variational level set models (CV, IVC, LIF, MCV, and MLCV), and (3) the integration of variational level set and clustering (Samson's model, VFCMS$_1$, and VFCMS$_2$).

4.1. The Choice of Parameters. For the choice of the initial level set function, under the combined effects of the clustering energy and internal energy, the choice of the initial level set function is very flexible. In our experiments, the initial level set functions are all chosen as $\phi_i(\mathbf{x}) = 1$ $(i = 1, \ldots, k)$. We also tested our model by using other initial level set functions, such as $\phi_i(\mathbf{x}) = 0$, signed distance function, and piecewise constant function. We found that our model using these different initial level set functions can all get correct image segmentation. We adopt a simple method to choose the initial cluster centers, which is stated as follows. Let $m = \min_{\mathbf{x}\in\Omega} f(\mathbf{x})$, $M = \max_{\mathbf{x}\in\Omega} f(\mathbf{x})$, and $h = (M - m)/k$; then

$$c_i = \frac{\sum_{\mathbf{x}\in\Omega_i} f(\mathbf{x})}{|\Omega_i|}, \tag{36}$$

where $\Omega_i = \{\mathbf{x} \in \Omega : m + (i-1)h \le f(\mathbf{x}) < m + ih\}$.

The parameter κ is a weighting parameter to measure the penalization for the formation of a vacuum and regions overlapping, which has a very important effect on the performance of the proposed model. So the value of κ should not be very small. In all experiments, we set $\kappa = 50$. We also find that for a wide range of κ over 50 (e.g., from 50 to 100), there seem to be no apparent changes in the results. The parameter σ adjusts the degree of smoothing. If it is too small, we cannot obtain good segmentation results due to the effect of the noises. Conversely, if σ is too large, the clustering boundaries will deviate from the image boundaries due to the oversmoothing of the image. How to choose an optimal smoothing parameter σ is still an "open question." In this paper, we adopted the "trial and error" technique to determine the value of smoothing parameter σ. In the experiments, if the image is corrupted by mixed 0.5% or 1% Salt and Pepper, Gaussian, and Speckle noise, we set $\sigma = 2$ and if the image is corrupted by 1.5% or 2% mixed noise, we set $\sigma = 2$. In order to obtain the optimal segmentation under the case of σ being fixed, the choice of parameter α is very important in the proposed model. For the FCMS$_1$, FCMS$_2$, GFCMS, VFCMS$_1$, and VFCMS$_2$ clustering models, the parameter α controls the weight of the spatial constraints. In the experiments, we still adopt "trial and error" technique to determine the value of parameter α. The detail of the choice of α is presented in Section 4.2. For the other parameters, we set $\lambda = 0.1$ and $\gamma = 1$.

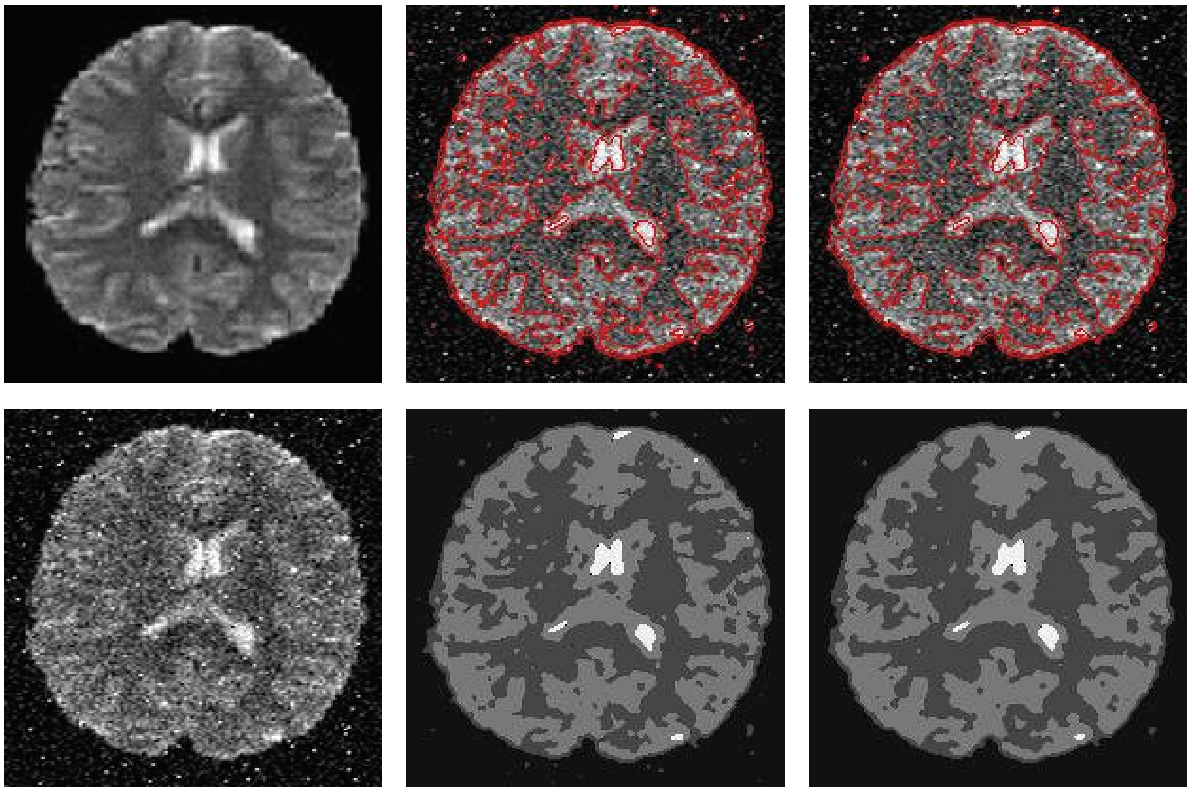

(a) Original image and its noisy version (b) $VFCMS_1$ (c) $VFCMS_2$

FIGURE 15: Segmentation results on a CT image with mixed 2% Salt and Pepper, Gaussian, and Speckle noise (cluster number $k = 4$).

4.2. Image Clustering Segmentation

Example 1 (the clustering segmentation of noisy synthetic images). Figure 1 shows the segmentation results of a synthetic image corrupted by 1% Salt and Pepper, Gaussian, and Speckle noise simultaneously. This image with 128×128 pixels contains two clusters (i.e., object and background). Experiment results show that FCM clustering, CV model, LIF model, and Samson's model cannot segment image well due to the effect of the noise. Since RBACM model utilizes the global image intensities inside and outside the contour, it can get better segmentation result. $FCMS_1$, $FCMS_2$, and GFCMS model also can get good segmentation due to the introduction of spatial information. However, we find that $FCMS_2$ and GFCMS clustering have fewer pixels being misclassified than $FCMS_1$. This is because $FCMS_1$ is implemented by median filtering, while $FCMS_2$ is implemented by mean filtering and GFCMS replaces the European distance with Gaussian kernel-induced distance. From Figures 1(n)–1(q), we can see that the proposed $VFCMS_1$ and $VFCMS_2$ models both can give us good segmentation. This is because we introduce the block-based term in the functional, except for spatial constraints. The last two plots show the surface plot for the convergent level set functions of $VFCMS_2$ model, respectively.

We take a set of values for α to test its performance in $FCMS_1$, $FCMS_2$, GFCMS, $VFCMS_1$, and $VFCMS_2$ clustering models. Figure 2(a) shows the comparisons of classification errors of these models under different values of α on the synthetic two-phase image shown in Figure 1(a). From Figure 2(a), as α increases, the numbers of misclassified pixels of all five models firstly reduce. $FCMS_1$, $FCMS_2$, and GFCMS reach minima between $\alpha = 2.8$ and $\alpha = 3.2$, and $VFCMS_1$ and $VFCMS_2$ reach minima when α in the interval of $[1.4, 3.0]$. From Figure 2(a), we note that as α continues to increase, the numbers of misclassified pixels of all five models will increase. In the first experiment (i.e., Figure 1), we set $\alpha = 2.2$ in $VFCMS_1$ and $VFCMS_2$, and set $\alpha = 2.8$ in $FCMS_1$, $FCMS_2$, and GFCMS.

Figure 3 shows segmentation results of the synthetic two-phase image corrupted by 2% Salt and Pepper, Gaussian, and Speckle noise simultaneously. For the choice of α, similarly, we take a set of values for α to test its performance. Figure 2(b) shows the comparisons of classification errors of $FCMS_1$, $FCMS_2$, GFCMS, $VFCMS_1$, and $VFCMS_2$ clustering models under different values of α. We obtain similar conclusions to the first experiment (see Figure 2(a)). From Figure 2(b), we set $\alpha = 3$ in $VFCMS_1$ and $VFCMS_2$, and set $\alpha = 3.2$ in $FCMS_1$, $FCMS_2$, and GFCMS. From Figure 3, we can clearly see that compared with the other models, the proposed models can achieve obvious predominance when image is corrupted by strong noise.

Figure 4 shows the segmentation results of a synthetic three-phase image corrupted by 0.5% Salt and Pepper, Gaussian, and Speckle noise. This image with 128×128 pixels contains three clusters. In the experiments, the parameters

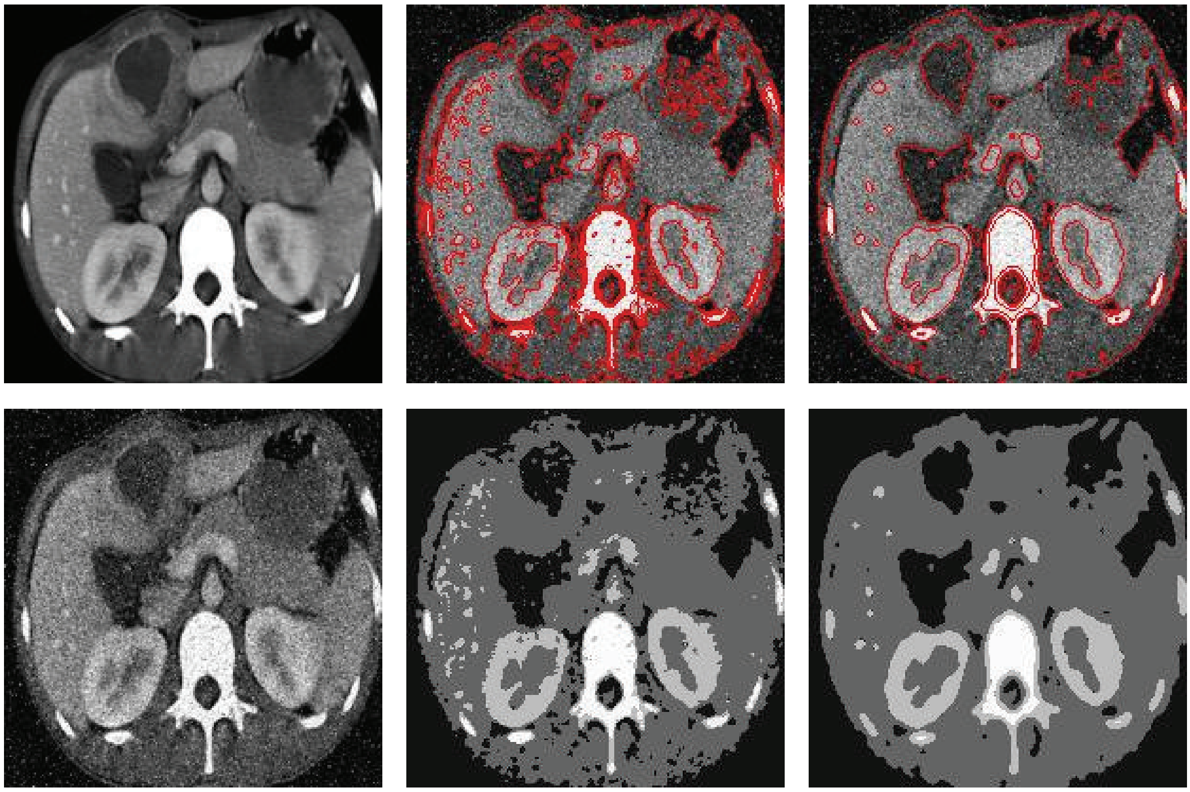

(a) Original image and its noisy version (b) $VFCMS_1$ (c) $VFCMS_2$

FIGURE 16: Segmentation results on a CT image with mixed 2% Salt and Pepper, Gaussian, and Speckle noise (cluster number $k = 4$).

are set as $\alpha = 2$ in $VFCMS_1$ and $VFCMS_2$, and $\alpha = 2.4$ in $FCMS_1$, $FCMS_2$, and GFCMS. Here, we add comparisons with MCV and MLCV which are both multiphase segmentation models. Experiment results show that FCM clustering, CV model, LIF model, and Samson's model cannot segment image well. Although RBACM is more robust to noise, it is a two-phase segmentation and segments this three-phase image into two parts. $FCMS_1$, $FCMS_2$, GFCMS, MCV, MLCV, $VFCMS_1$, and $VFCMS_2$ perform better on the visual effect than other methods. The last three plots show the surface plot of the convergent level set functions of $VFCMS_2$, respectively.

Figure 5 shows the segmentation results of the synthetic three-phase image corrupted by 1.5% Salt and Pepper, Gaussian, and Speckle noise. We set $\alpha = 2.6$ in $VFCMS_1$ and $VFCMS_2$, and $\alpha = 3$ in $FCMS_1$, $FCMS_2$, and GFCMS. From experiment results, we can see that FCM clustering, CV model, LIF model, and Samson's model still do not segment image well. It is observed that $FCMS_1$ also cannot achieve satisfactory result in the case of image being corrupted by strong noise. This is because it is implemented by median filtering. Similar to Figure 4, $FCMS_2$, GFCMS, MCV, MLCV, $VFCMS_1$, and $VFCMS_2$ can achieve better segmentation.

Table 1 gives us the segmentation accuracy (SA) of the models on the images shown in Figures 1(a), 3(a), 4(a), and 5(a), where SA is defined as the total number of correctly classified pixels by the total number of all pixels [16]. By quantitative comparison of SA, the proposed $VFCMS_1$ and $VFCMS_2$ can achieve more accurate segmentation than the other models under different noise levels.

Example 2 (the clustering segmentation of noisy plane image). Figure 6 presents the comparison results (clustering into 2 clusters) on a plane image corrupted by 2% Salt and Pepper, Gaussian, and Speckle noise simultaneously. It is obvious that FCM, CV, LIF, and Samson's model cannot segment image well. $FCMS_1$, $FCMS_2$, GFCMS, and GBACM can achieve better segmentation than FCM, CV, LIF, and Samson's model. Among these ten models, the proposed $VFCMS_1$ and $VFCMS_2$ can obtain the superior segmentation, and only a few pixels are misclassified. Furthermore, we find that $VFCMS_2$ can give us a better segmentation than $VFCMS_1$, This is because $VFCMS_1$ is implemented by median filtering, and $VFCMS_2$ is implemented by mean filtering. We conclude that if the test data is corrupted by strong noise, $VFCMS_2$ can get better segmentation than $VFCMS_1$ in general. The last two plots show the surface plot of the convergent level set functions of $VFCMS_2$.

Figure 7 presents the comparison results (clustering into 3 clusters) on the noisy plane image corrupted by 2% mixed Salt and Pepper, Gaussian, and Speckle noises. This image contains two low-contrast regions (i.e., background region and the shadow region of plane). Furthermore, these two regions are contaminated by strong noises. We would like to segment noisy plane image into 3 parts and discriminate

Table 1: SA % of twelve models on noisy synthetic image.

	Figure 1(a)	Figure 2(a)	Figure 4(a)	Figure 5(a)
FCM	90.34	86.45	87.32	85.47
$FCMS_1$	99.01	97.87	98.84	98.74
$FCMS_2$	99.32	99.24	99.14	99.07
GFCMS	99.48	99.43	99.23	99.15
CV	89.75	87.27	68.14	68.11
LIF	72.34	71.45	62.32	61.46
RBACM	96.57	96.53	70.34	70.28
MCV			99.34	99.32
MLCV			99.47	99.44
Samson's model	85.89	83.42	96.42	95.47
$VFCMS_1$	99.53	99.47	99.45	99.43
$VFCMS_2$	99.82	99.78	99.64	99.62

these two low-contrast regions. From this figure, we can see that FCM, $FCMS_1$, $FCMS_2$, GFCMS, MCV, MLCV, and Samson's model cannot distinguish these two low-contrast regions well. While the proposed $VFCMS_1$ and $VFCMS_2$ model can obtain the good segmentation results on these two low-contrast regions due to the use of block-based energy and variational level set scheme. The last three plots show the surface plot of the convergent level set functions of $VFCMS_2$.

Example 3 (the clustering segmentation of real images corrupted by mixed noise). Finally, to show the practicability and validity of the proposed model, different kinds of real images corrupted by mixed Salt and Pepper, Gaussian, and Speckle noise are tested. Compared with the synthetic images, these real images contain much more complex boundaries, weak boundaries, inhomogeneous regions, and low-contrast regions. Figures 8, 9, and 10 show the segmentation results of the images which are segmented into two clusters. Figures 11, 12, and 13 show the segmentation results of the images which are segmented into three clusters. The segmentation results of the images that are segmented into four clusters are shown in Figures 14, 15, and 16. From Figures 8–16, we can clearly see that the proposed model can overcome the influence of noise and obtain the excellent segmentation results for different kinds of noisy real images.

5. Conclusions

In this paper, based on the Samson's work and FCMS clustering, we proposed a new variational level set model combined with FCMS for image clustering segmentation. In addition, a block-based energy was incorporated into the energy functional, which enables the proposed models robust to the noise. Some synthetic and real noisy images with different noise levels were employed to compare the performance of 12 models. Experimental results show that the proposed model has a superior performance among these methods. And different kinds of real noisy image were also used to show the practicability and validity of the proposed model.

The experimental results reported in this paper show that the proposed VFCMS model is very effective for noise image clustering segmentation. This model can also be improved by incorporating other FCMS-based clustering algorithms, for example, Kernel-induced FCMS proposed by Chen and Zhang [16] or Gaussian Kernel-induced FCMS proposed by Yang and Tsai [17], and so forth. We note that in passing our model still has some drawbacks, such as (1) it is a semisupervised image clustering segmentation and needs to predetermine the clustering numbers; (2) Key parameters such as α weighting spatial term and σ controlling Gaussian smoothing are determined by human-machine interaction; (3) the proposed model is more complex and takes more computing time than some other classical variational level set model, such as CV, LBF, LIF, and MCV. So, the proposed model has major drawback of weak real-time performance. Our further works will include autoselecting parameters, adaptive determination of the clustering number, and improving real-time capability of VFCMS.

Conflict of Interests

The author declares that there is no conflict of interests regarding the publication of this paper.

References

[1] T. F. Chan, B. Y. Sandberg, and L. A. Vese, "Active contours without edges for vector-valued images," *Journal of Visual Communication and Image Representation*, vol. 11, no. 2, pp. 130–141, 2000.

[2] C.-J. He and L.-M. Tang, "Anisotropic diffusion of halting speed fields in geometric active contour model," *Journal of Software*, vol. 18, no. 3, pp. 600–607, 2007.

[3] C. Li, R. Huang, Z. Ding, J. C. Gatenby, D. N. Metaxas, and J. C. Gore, "A level set method for image segmentation in the presence of intensity inhomogeneities with application to MRI," *IEEE Transactions on Image Processing*, vol. 20, no. 7, pp. 2007–2016, 2011.

[4] B. Liu, J.-H. Huang, X.-L. Tang, J.-F. Liu, and Y.-T. Zhang, "Combining global probability density difference and local gray level fitting for ultrasound image segmentation," *Acta Automatica Sinica*, vol. 36, no. 7, pp. 951–959, 2010.

[5] D. Mumford and J. Shah, "Optimal approximations by piecewise smooth functions and associated variational problems,"

Communications on Pure and Applied Mathematics, vol. 42, no. 5, pp. 577–685, 1989.

[6] T. F. Chan and L. A. Vese, "Active contours without edges," *IEEE Transactions on Image Processing*, vol. 10, no. 2, pp. 266–277, 2001.

[7] K. Zhang, L. Zhang, H. Song, and W. Zhou, "Active contours with selective local or global segmentation: a new formulation and level set method," *Image and Vision Computing*, vol. 28, no. 4, pp. 668–676, 2010.

[8] C. Li, C.-Y. Kao, J. C. Gore, and Z. Ding, "Implicit active contours driven by local binary fitting energy," in *Proceedings of the IEEE Computer Society Conference on Computer Vision and Pattern Recognition (CVPR '07)*, pp. 1–7, Washington, DC, USA, June 2007.

[9] K. Zhang, H. Song, and L. Zhang, "Active contours driven by local image fitting energy," *Pattern Recognition*, vol. 43, no. 4, pp. 1199–1206, 2010.

[10] L. A. Vese and T. F. Chan, "A multiphase level set framework for image segmentation using the Mumford and Shah model," *International Journal of Computer Vision*, vol. 50, no. 3, pp. 271–293, 2002.

[11] S. Gao and Y. Yan, "Brain MR image segmentation via a multiphase level set approach," *Journal of Information & Computational Science*, vol. 16, no. 9, pp. 4705–4711, 2012.

[12] J. C. Dunn, "A graph theoretic analysis of pattern classification via Tamura's fuzzy relation," *IEEE Transactions on Systems, Man and Cybernetics*, vol. 4, no. 3, pp. 310–313, 1974.

[13] J. C. Bezdek, "A convergence theorem for the ISODATA clustering algorithm," *IEEE Transactions on Pattern Analysis and Machine Intelligence*, vol. 2, no. 1, pp. 1–8, 1980.

[14] H. Cao, H.-W. Deng, and Y.-P. Wang, "Segmentation of M-FISH images for improved classification of chromosomes with an adaptive fuzzy C-means clustering algorithm," *IEEE Transactions on Fuzzy Systems*, vol. 20, no. 1, pp. 1–8, 2012.

[15] M. N. Ahmed, S. M. Yamany, N. Mohamed, A. A. Farag, and T. Moriarty, "A modified fuzzy C-means algorithm for bias field estimation and segmentation of MRI data," *IEEE Transactions on Medical Imaging*, vol. 21, no. 3, pp. 193–199, 2002.

[16] S. Chen and D. Zhang, "Robust image segmentation using FCM with spatial constraints based on new kernel-induced distance measure," *IEEE Transactions on Systems, Man, and Cybernetics B*, vol. 34, no. 4, pp. 1907–1916, 2004.

[17] M.-S. Yang and H.-S. Tsai, "A Gaussian kernel-based fuzzy c-means algorithm with a spatial bias correction," *Pattern Recognition Letters*, vol. 29, no. 12, pp. 1713–1725, 2008.

[18] S. R. Kannan, S. Ramathilagam, A. Sathya, and R. Pandiyarajan, "Effective fuzzy c-means based kernel function in segmenting medical images," *Computers in Biology and Medicine*, vol. 40, no. 6, pp. 572–579, 2010.

[19] H. Q. Liu, F. Zhao, and L. C. Jiao, "Fuzzy spectral clustering with robust spatial information for image segmentation," *Applied Soft Computing*, vol. 12, no. 11, pp. 3636–3647, 2012.

[20] Y. He, M. Yousuff Hussaini, J. Ma, B. Shafei, and G. Steidl, "A new fuzzy c-means method with total variation regularization for segmentation of images with noisy and incomplete data," *Pattern Recognition*, vol. 45, no. 9, pp. 3463–3471, 2012.

[21] C. Samson, L. Blanc-Féraud, G. Aubert, and J. Zerubia, "Level set model for image classification," *International Journal of Computer Vision*, vol. 40, no. 3, pp. 187–197, 2000.

[22] C. Li, C. Xu, C. Gui, and M. D. Fox, "Level set evolution without re-initialization: a new variational formulation," in *Proceedings of the IEEE Computer Society Conference on Computer Vision and Pattern Recognition (CVPR '05)*, pp. 430–436, IEEE Computer Society Press, June 2005.

[23] K. Zhang, L. Zhang, H. Song, and D. Zhang, "Reinitialization-free level set evolution via reaction diffusion," *IEEE Transactions on Image Processing*, vol. 22, no. 1, pp. 258–271, 2013.

[24] Q. Chen, P. Montesinos, Q. S. Sun, P. A. Heng, and D. S. Xia, "Adaptive total variation denoising based on difference curvature," *Image and Vision Computing*, vol. 28, no. 3, pp. 298–306, 2010.